NBSIR 88-3798

Mechanical Property Enhancement in Ceramic Matrix Composites

S.W. Freiman, T.W. Coyle, E.R. Fuller, Jr.,
P.L. Swanson, D.C. Cranmer, and W. Haller

U.S. DEPARTMENT OF COMMERCE
National Bureau of Standards
Institute for Materials Science and Engineering
Electrical/Electronics Ceramics Group
Ceramics Division
Gaithersburg, MD 20899

April 1988

Interim Report

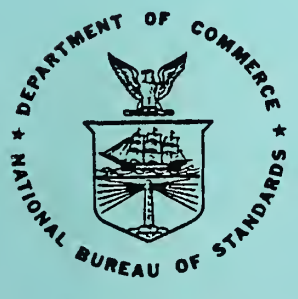

U.S. DEPARTMENT OF COMMERCE
NATIONAL BUREAU OF STANDARDS

NBSIR 88-3798

MECHANICAL PROPERTY ENHANCEMENT IN CERAMIC MATRIX COMPOSITES

S.W. Freiman, T.W. Coyle, E.R. Fuller, Jr.,
P.L. Swanson, D.C. Cranmer, and W. Haller

U.S. DEPARTMENT OF COMMERCE
National Bureau of Standards
Institute for Materials Science and Engineering
Electrical/Electronics Ceramics Group
Ceramics Division
Gaithersburg, MD 20899

April 1988

Interim Report

U.S. DEPARTMENT OF COMMERCE, C. William Verity, *Secretary*
NATIONAL BUREAU OF STANDARDS, Ernest Ambler, *Director*

MECHANICAL PROPERTY ENHANCEMENT IN CERAMIC MATRIX COMPOSITES

S. W. Freiman, T. W. Coyle, E. R. Fuller Jr., P. L. Swanson,
D. C. Cranmer, and W. Haller

Ceramics Division
National Bureau of Standards
Gaithersburg, MD 20899

M. J. Koczak, M. Barsoum, U. V. Deshmukh, and T. R. Palamides

Department of Materials Engineering
Drexel University
Philadelphia, PA 19104

INTERIM REPORT

This program supported by the Strategic Defense Initiative
Office/Innovative Science and Technology under ONR Contract
CONTRACT NUMBER: N00014-86-F-0096

April 30, 1988

Mechanical Property Enhancement
In Ceramic Matrix Composites

Table of Contents

ABSTRACT

The interfacial strength between AVCO SCS-6 filaments and a borosilicate glass matrix was measured using an indentation push-in technique. Crack-filament interactions were investigated using a fracture mechanics technique (DCDC). An ultraviolet curing technique, coupled with hot pressing was developed to prepare SiC filament-borosilicate glass composites.

MECHANICAL PROPERTY ENHANCEMENT IN CERAMIC MATRIX COMPOSITES

BACKGROUND

The key parameters responsible for the stress-strain behavior and damage tolerance of fiber-reinforced ceramic composites are the fracture toughness of the matrix, the strength of the fiber/matrix interface, and the properties and distribution of the fibers themselves. Increases in the fracture resistance of the matrix and the strength of the interface are predicted to lead to an increase in the stress at which the matrix begins to microcrack. Balanced against this increase in microcracking stress is the necessity for maintaining some degree of fiber pullout in order to achieve the desired stress-strain behavior in the composite. Quantitative experimental verification of the models developed to explain composite fracture (1-5) has not yet been obtained.

The primary objective of this program is to experimentally determine the relationships between the fracture behavior of fiber-reinforced ceramic composites, the properties of the individual components, and the interface between the fiber and the matrix. A second objective is to establish mechanical test procedures appropriate for these composite systems. The increased understanding of the fracture process will be used to develop strong/damage tolerant materials.

The initial composite system chosen for study in this program was a borosilicate glass matrix reinforced with continuous SiC filaments (SCS-6, AVCO Corp.).* This system was chosen for a number of reasons including ease of fabrication, thermal expansion match between fiber and matrix, and the

*AVCO Corporation, Waltham, Massachusetts

handlability and reproducibility of fibers. The work to date is divided into three parts: 1) measurement of the interfacial fiber/matrix strength, 2) determination of the effect of fibers in retarding crack extension, and 3) development of composite fabrication capability. Results of each of these activities are described in the following sections.

RESULTS

Interfacial Strength Measurement

The method used to determine the strength of the fiber/matrix interface is based on the indentation technique proposed by Marshall (6). A Vickers hardness indenter is used to apply a force, P, to a fiber parallel to the fiber axis in a polished cross section of the composite. The method is an extension of Marshall's technique in that the indenter is instrumented to measure both the load applied to the fiber as well as the displacement of the diamond tip. The load-displacement curves can be used to calculate interfacial strength.

The experimental load-displacement curves must be corrected to account for penetration of the indenter diamond into the matrix. During the initial part of the loading, the diamond tip penetrates the surface of the fiber, while at the same time, the fiber begins to slip in the matrix. To determine the displacement, u, of the fiber surface relative to the matrix, the penetration of the indenter, a, must be subtracted from the total displacement. This penetration is given through Equation 1.

$$a = (F/2H_f)^{1/2}/\mathrm{Tan}\ \Phi \qquad (1)$$

where F is the force applied to the fiber, H_f is the fiber hardness, and Φ is the half-angle (74°) of the Vickers indenter. Initially, all of the applied load from the indenter acts on the fiber, F = P. As the fiber slips into the

matrix, the edges of the indenter penetrate the surrounding matrix. Penetration begins at d = 2R, where d is the length of the diagonal made by the indenter in the fiber surface, and R is the fiber radius. The portion of the load now carried by the matrix must be subtracted from the measured load.

The calculation of the interfacial strength, τ, when fiber slippage occurs through the entire thickness of the sample, i.e., for thin samples, is relatively straightforward if it is assumed that the applied shear stress is constant along the interface. When τ is constant, a simple force balance yields:

$$\tau = F/2\pi Rt \tag{2}$$

where t is the specimen thickness. In this case, the applied load should be constant for displacements less than that which causes the indenter to contact the matrix.

The calculation becomes more complicated when the sample thickness is larger than the fiber slippage length, ℓ . Marshall (6) has presented an approximate analysis for the case of $t >> \ell$. Stress concentrations and Poisson's ratio effects are ignored, and τ is assumed to be independent of position and slippage distance. If axial compressive stresses in the fiber are neglected, then:

$$F^2 = \frac{4\pi^2 R^3 E_f}{[1 - \pi B(R/\ell)^2]^2} \tau u \tag{3}$$

where E_f is the Young's modulus of the fiber and B is a constant ≈ 1 (6).

A plot of F^2 versus u following Equation 3 is shown in Figure 1 for a Nicalon SiC fiber in a glass ceramic (LAS-III) matrix.** The slope of this curve is proportional to τ. The curve is essentially linear over the range

---

**United Technologies Research Center, East Hartford, CT

0.25 μm < u < 1.25 μm, with a slope of 3.41 x 10^4 N^2/m. The fiber radius was 8.5 μm and E_f = 200 GPa. τ was calculated to be 7.0 MPa, in agreement with other measurements (6).

The interfacial strength between AVCO SCS-6 monofilaments and a borosilicate glass matrix was also measured. Thin (0.16 mm) specimens were cut from a larger billet so that the simpler analysis shown in Equation 2 could be employed as well as to limit the force required to displace the filament. Values of the debonding (i.e., initial values) shear strength of 0.8 to 1.0 MPa were measured in this way.

CRACK-FIBER INTERACTIONS

Fracture Mechanics Procedure

This investigation made use of a test known as the Double Cleavage Drilled Compression (DCDC) procedure. The DCDC specimen has been used to study crack growth in brittle materials for several years (7). The DCDC specimen (Figure 2) is a rectangular column having a center hole drilled through the thickness such that the bore axis is perpendicular to the width of the specimen. The DCDC specimen is unique in that when the column is loaded in axial compression, cleavage cracks initiate simultaneously from the top and bottom of the drilled hole and grow in a stable manner as the load is increased.

Some characteristic features which make the DCDC specimen desirable are:

A. stable centerline propagation of cracks without the aid of guide grooves,

B. the decaying K_I field present under remote load conditions,

C. well defined crack plane perpendicular to the direction of propagation in a cleavage opening, and

D. specimen loading which eliminates detrimental torsion or bending often present in other fracture mechanics specimens.

In all cases the stress intensity factor K_I has the general form:

$$K_I = f(c/r)\beta C^{1/2} \tag{4}$$

where: $f(c/r)$ = a dimensionless geometric coefficient,

c = the crack length.

r = the hole radius, and

β = the nominal applied stress.

The dimensionless geometric coefficient was experimentally determined by plotting normalized stress versus normalized crack length. A linear regression was performed to determine the stress intensity factor as a function of crack length. The equation for the dimensionless geometric coefficient used in this experiment was:

$$f(c/r) = 0.138(c/r) + 1.852 \tag{5}$$

The DCDC specimen was used to investigate the effects of SiC filaments on the stress intensity necessary to drive a crack. SiC filaments (SCS-6) were placed at two distances from the center hole (Figure 3). It was hypothesized that the presence of the filaments would cause K_I to vary as a function of crack length. If a propagating crack bows around the isolated fiber and passes it without fiber fracture occurring, the fiber then acts as a bridge between the two planar surfaces, inhibiting their separation and causing the stress intensity factor to increase. In this study the bridging force produced by the filaments was determined as a point force, and not a surface shear stress, due to the unmeasured length of fiber pull-out between the crack surfaces. This bridging, or traction force, is a function of the frictional bonding between the fiber surface and the glass matrix.

Assuming that the critical stress intensity, K_{IC}, is equal to the fracture toughness of the glass at the tip of the crack (this is valid in the absence of environmentally assisted slow crack growth), a simple mathematical relationship can be stated:

$$K_{tip} = K_{IC} = K_{applied} + K_{traction} \tag{6}$$

where $K_{applied}$ is the stress intensity for a given applied stress, and $K_{traction}$ is the stress intensity imposed by the fiber.

By obtaining $K_{applied}$ from Equation (4) and knowing K_{IC} for borosilicate glass (0.77 $MPa \cdot m^{1/2}$) from previous experiments, $K_{traction}$ was determined. $K_{traction}$ can be related to a point force acting at a distance δ behind the crack tip, by the following equation (8):

$$K_{traction} = -(\sqrt{2})F/(\pi\delta)^{3/2} \tag{7}$$

where F is a point force on the fiber.

Stress-wave fractography (9) was used to characterize the propagation of the crack front and to make crack velocity measurements. By introducing a periodic stress oscillation perpendicular to the direction of the maximum principal tensile stress, optically observable undulations are produced on the fracture surface. The spacing between the undulations gives a measure of the crack growth rate.

Experimental Procedure

The DCDC specimen was fabricated by the diffusional bonding of two borosilicate*** glass plates. The specimen preparation route is illustrated in Figure 4. Four 140-μm-diameter SiC filaments were placed between the plates prior to bonding. A U-shaped stainless steel bracket with notched

***CGW 7740, Corning Glass Works, Corning, NY

grooves cut cross-wise was used to ensure proper fiber alignment within the matrix as well as to provide specimen reproducibility.

The SiC fibers were given an oxidation treatment (950 ^{o}C for 4 hrs.) prior to their incorporation in the matrix in order to minimize the presence of bubbles occurring along the fiber/matrix interface during sintering. This treatment is believed to promote the formation of a protective layer of SiO_2 on the fiber surface, which prevents deleterious reactions from occurring during consolidation, but can also influence the interfacial strength between the fiber and the glass.

The diffusional bonding operation was conducted in a tube furnace in air at $\approx$ 850 ^{o}C for 25-30 minutes. This fabrication route caused a thin crystalline layer to form on all free surfaces. (No effect of this thin crystalline layer on crack growth was noted.) After bonding, the specimens were annealed and polished. The final preparation step was to bore a hole through the thickness of the specimen.

In the stress-wave fractography study, a transducer was mounted to the lower end of the DCDC specimen with vacuum grease. Resonance frequencies were observed by monitoring the electrical output of the transducer. The signal decided upon for the transducer was an 80-90 KHz sine wave having a maximum of 30 V peak-to-peak. That signal was gated with a burst frequency of 5 KHz which consisted of 24% of the low frequency period. This signal gave clear undulations in most regions along the crack plane. An illustration detailing the arrangement of the equipment set-up and schematic of the wiring is found in Figure 5.

The DCDC specimens were tested in compression with a screw-driven mechanical testing machine (Figure 6). The crosshead was operated at a

constant displacement rate of 0.005 cm/min for all specimens. A double-cup ball joint was placed between the specimen and the crosshead to minimize the possibility of misalignment during testing. Polarized light was used to follow the crack tip. Interference fringes in the polarized field were enhanced with quarter-wave plates and complete documentation of the crack route was made using 35 mm photography.

Results and Discussion

Force versus crosshead displacement curves were plotted having incrementally numbered marks corresponding to photographs taken of the propagating crack through the polarized field of view. The applied stress intensity was determined from measurements of the applied load and the crack length through the use of Equations 4 and 5.

In Figure 7 the applied stress intensity is plotted versus the normalized crack length. Once the crack passes the filament, indicated by the dark vertical line, the applied stress intensity on the propagating crack increased monotonically to a value ≈ 20% higher than that for the base glass. This increase is hypothesized to be due to the bridging effect of the filament. As noted earlier, the bridging force due to the filament can be estimated via Equation 7. The bridging force is produced by the frictional adhesion of the filament to the matrix. The maximum force is reached prior to fiber pull-out or fracture. A bar graph illustrating the variation in point force between specimens is shown in Figure 8. Specimens C and E are not indicated in this figure because they were misaligned during testing. The calculated force ranges from 29 N to 63 N with specimens A and B identical at 29 N and specimen D showing the highest point force of 63 N.

Figure 9 shows a photomicrograph of the fracture plane in the vicinity of a SiC fiber. It should be noted that most fibers did not fracture at the crack plane, indicating that some pull-out had occurred. Figure 10 gives a closeup of the formation of a thin alpha-cristobalite crystalline layer which formed on all free surfaces during the diffusional bonding process. This thin crystalline layer did not appear to affect fracture in the vicinity of the fiber.

The interaction of the crack front with the fiber can be seen in Figures 11 and 12. The leading edge of the crack plane appears to bow around the fiber, leaving striations in its wake. Once past the fiber, the propagating crack hesitates, leaving thin demarcations on the fracture surface.

Photomicrographs taken during the stress-wave fractography experiment are shown in Figures 13 and 14. Figure 13 shows the onset of fracture, which can be traced to the edge of the black region toward the center of the photomicrograph. Figure 14 is a higher magnification of the undulations occurring along the fracture surface from which crack velocities can be determined. In this experiment, the velocity of the crack decreased from 6.0-8.0 x 10^{-5} m/s in the bulk of the specimen to 1.5-3.0 x 10^{-5} m/s near the fiber, indicating the inhibiting effect of the fiber on crack growth.

Conclusions

* The DCDC specimen was determined to be a viable specimen for the characterization of crack/fiber interactions in ceramic matrix composites.

* The incorporation of SiC fibers in the DCDC specimen caused the applied stress intensity to be increased by approximately 20%.

* Stress-wave fractography provided insight into the crack front behavior and crack velocity. The velocities were 6.0-8.0 x 10^{-5} m/s in the borosilicate glass region of the specimen and 1.5-3.0 x 10^{-5} m/s in the immediate vicinity of the fiber.

COMPOSITE PROCESSING

Most composite processing technology is proprietary; thus, some effort was directed towards establishing a processing route to make composites in a reproducible way. Consolidation temperature and pressure were identified as the two most important parameters in producing fully dense composites. The raw materials for this research were 7740 glass powder supplied by Corning Glass Works and AVCO SCS-6 SiC monofilaments. The glass powder has a nominal composition reported by Corning to be 81% SiO_2, 2% Al_2O_3, 13% B_2O_3, and 4% Na_2O. The SiC monofilaments are produced by a chemical vapor deposition (CVD) process. Each filament consists of a 33 μm diameter graphite core surrounded by fine grains of β -SiC, which in turn is coated with carbon (AVCO) (Fig. 15). The smooth graphite coating increases filament strength by eliminating surface flaws and closing the open grain boundaries on the surface.

Because of the tendency of the glass powder to crystallize in a temperature range 800-900 ^{o}C, processing temperatures were kept below 800 ^{o}C. Above 900 ^{o}C the glass flows easily, and as a result can get squeezed into the die clearances on application of pressure, causing die wear and making composite removal difficult.

The composites were hot pressed in a carbon-carbon die in an argon atmosphere. The punches were made of high strength graphite. Molybdenum

sheets were used in regions that came in direct contact with the glass, since borosilicate glass does not stick to molybdenum.

The sequence of composite fabrication was as follows. The die with the green composite in the cavity was assembled outside the hot press; then the die assembly was placed in the hot press, aligned with the pressing rams and held in place by the application of sufficient pressure. The hot press chamber was then evacuated using a mechanical pump and flushed with helium at least three times. Helium was kept flowing for the entire period of operation to minimize die assembly oxidation. The die was heated to the required temperature at a rate of 5 ^{o}C/min. After the die was at the required temperature for about 15 to 30 minutes, pressure was applied. The reason for this temperature hold is to allow the die interior to attain the surface temperature. In the assembly that was used, only the surface temperature of the die could be monitored. The pressure was applied in steps with consolidation being monitored by LVDT movement which recorded the ram displacement. Usually when the LVDT signal leveled off, it indicated maximum possible consolidation at that temperature and pressure. Caution must be exercised though because at high temperature the glass is less viscous, so that under the applied pressure it may continue to flow in the die clearances. As a result the LVDT could continue to register ram displacement. A typical processing parameter chart is shown in Figure 16.

Initial composites were fabricated from dry powders, i.e., no wet binder was used. Monofilaments ≈ .5-m-long were cut from the spool and hand layed up to form a 13-mm-wide tape. This tape was cut into ≈ 40-mm-long sections, the filaments being held by tape at the ends. Glass powder was poured into the bottom of the die cavity and spread evenly; a section of filament tape was

placed on it. This process was repeated to build up the composite. The top layer was glass. As this experiment was designed to optimize the processing parameters, viz., temperature and pressure, only a few layers of filaments were used.

Green composites fabricated as outlined above were hot pressed at 800 ^{o}C, 700 ^{o}C and 675 ^{o}C under a final pressure of 6.8 MPa. To monitor the consolidation, the bulk density of the composite was measured using Archimedean principles (Table 1). As can be seen, maximum density was obtained at around 700 ^{o}C. Subsequent composites were hot pressed at a slightly higher temperature.

The next step in the process was to increase the filament volume fraction in the composites. The composites were manufactured exactly as above, except that the amount of glass that was poured between the successive filament section was considerably reduced. After assembling the die, the composites were hot pressed at 750 ^{o}C under 6.8 MPa pressure.

There are drawbacks to this technique of composite manufacture. First, the resulting composite tends to be inhomogeneous in terms of filament spacing both within a row as well as between rows. The filament spacing within a row is controlled by the accuracy of the lay-up. The spacing between rows is controlled to an extent by the glass flow during hot pressing. Another factor contributing to inhomogeneity comes from unequal quantities of glass between filament layers. Secondly, the apparent volume fraction of the filaments in the composites is reduced, since there is excess glass at the top and bottom. In order to test these composites the excess glass at the surface must be removed. Thirdly, making composites by this technique is fairly labor intensive.

In order to overcome these problems, it was necessary to adopt a processing route in which the fibers are continuously coated by the matrix powders and can be wound at a desired spacing. A typical route is shown schematically in Figure 17. In this technique the fiber/yarn is unwound from the spool and passed through a flame to burn off the sizing. It is then passed through a slurry consisting of a fugitive organic binder, matrix powder, and a few additives such as wetting, dispersing and anti-foaming agents. The purpose of these additives is to facilitate good powder dispersion in the slurry. The coated fiber/yarn is then wound on a mandrel to form a tape. The tape is removed from the mandrel, cut to the size of the die cavity, and stacked according to requirement, viz., 0 degrees or 0/90 degrees. Next, this stack is transferred to a low temperature oven where the binder is burned out. It is essential to burn out the binder in the presence of air to remove all the carbonaceous matter from the matrix. It is also beneficial to increase the temperature after the burnout so that the matrix powder sinters slightly, which aids in handling. This "green" stack is put in the carbon mold and hot pressed in an inert atmosphere at the required temperature and pressure.

It may be noted that the crucial aspect of this technique is to evenly coat the fiber with the slurry. In the case of yarn, even though the wetting may not be good, capillary action helps in the dispersion of matrix powder among the individual fibers in the tow. The volume fraction of the fibers obtained is mainly dependent on the slurry "pick-up" by the yarn. The volume fraction can also be manipulated by changing the binder to matrix powder ratio, or by changing the drawing speed. It should be noted that the "pick-up" cannot be controlled precisely. This technique has been fairly well

established for the processing of composites with continuous fibers. Another technique very similar to the one noted above was also used to manufacture composites in this program. In this process the fiber is first wound on a mandrel at the desired spacing to make a tape. The tape is then removed from the mandrel and the slurry is hand painted. Further processing, viz., binder burnout and hot pressing, is the same as above. Several composites were made by this technique to demonstrate the process applicability.

The SCS-6 monofilaments used in this research have a carbon-rich surface making them non-wetting to glasses. Thus, when a monofilament is drawn through the slurry, the slurry film tends to break-up into a string of globules along the fiber length. This surface instability results from the effect of surface tension. The viscosity of the slurry dictates the amount of time it takes for the slurry film to bead. However, too thick a slurry cannot be used since it leaves a nonuniform film on the surface. Therefore the key in processing appears to be the "hardening time", i.e, the time to dry/harden the coating before it breaks up can be controlled by using a rapidly evaporating solvent for the binder. Experiments were also conducted with melt-binders such as agar-agar which were applied hot and solidified on cooling. This technique was successful but process optimization was rather tedious. Therefore, a set-up involving ultraviolet light curing was developed (Figure 18). The set-up consists of a cup with a small hole at the bottom, with a guide for centering the filament in the hole fixed on the top. The slurry, consisting of a dispersion of the matrix powder in an organic monomer, is poured into the cup. The slurry must be viscous to prevent it from running down through the bottom hole. The cup can be pressurized to make the slurry flow evenly. A filament is introduced through the top of the cup, passed

through the slurry, and the coated filament emerging from the bottom is exposed to ultraviolet radiation. This instantly polymerizes the monomer, thereby hardening the coating. The process can be operated continuously, and the coated filament can be wound on the mandrel at a desired spacing. The process is capable of reproducibly coating the monofilament. The amount of matrix that can be applied to the fiber surface can be controlled in two ways. First the ratio of glass to the monomer can be changed; second, the drawing speed can be varied to obtain different coating thicknesses. Thus, this process is more flexible and can be operated to obtain a range of monofilament volume fractions.

In order to prepare composites, the coated filament tape is layed up, sectioned to appropriate size, and stacked to obtain the composite thickness. The binder is burned off in air, and the green composite is hot pressed. Composites with SiC monofilament and borosilicate glass matrix have been successfully manufactured by this route. It is important to note that the same monomer can be used for any matrix. Thus, the technique can be used to manufacture almost any monofilament reinforced composite as long as the matrix is available as particulates.

SUMMARY

The three primary areas of research in this program are measurement of interfacial strengths, determination of crack-fiber interactions, and fabrication development for ceramic matrix composites. Significant progress has been achieved in all three areas.

1. An instrumented hardness machine has been used to measure the interfacial strengths between AVCO filaments and borosilicate glass. Values of the debonding strength of 0.8 to 1.0 MPa were determined.

2. The double cleavage drilled compression (DCDC) specimen was used to study crack-fiber interactions in this same SiC-borosilicate glass system. A fracture mechanics analysis demonstrated the role of the bridging filament in retarding crack propagation. The analysis also showed the quantitative relationship of the bridging force to the interfacial strength between filament and matrix.

3. An ultraviolet, polymer curing technique coupled with a hot pressing procedure was developed to prepare SiC monofilament-borosilicate glass composites.

FUTURE PLANS

A major effort during the coming year will be to determine effects of fiber surface modifications on both the interfacial strength as well as the crack fiber interactions in the SiC-borosilicate glass system. Various technique for surface modification will be employed, including coatings, oxidation, etc. Effects of thermal expansion differences between fiber and matrix will also be determined by varying the glass matrix composition. A portion of our effort during the coming year will be to develop tensile test procedures for these composites so that testing of the actual composites can be performed at both ambient and elevated temperatures. Nondestructive test techniques for detecting the onset of microcracking in these composites will be investigated.

REFERENCES

1. J. Aveston, G. A. Cooper, and A. Kelly, The Properties of Fibre Composites , pp. 15-26, National Physical Laboratory, Science and Technology Press Ltd., London, (1971)

2. J. Aveston and A. Kelly, J. Mat. Sci., 8, 352, (1973)

3. D. B. Marshall and A. G. Evans, J. Am. Ceram. Soc., 68, 225 (1985)

4. D. B. Marshall, B. N. Cox, and A. G. Evans, Acta Metall., 33, 2013 (1985)

5. B. Budiansky, J. W. Hutchinson, and A. G. Evans, J. Mech. Phys. Solids, 34, 167 (1986)

6. D. B. Marshall, Comm. Am. Ceram. Soc., 67, C-259 (1985)

7. C. Janssen, Tenth International Congress on Glass, 23, Kyoto, Japan (1974)

8. H. Tada, P. C. Paris, and G. R. Irwin, The Stress Analysis of Cracks Handbook, Del Research Corp., Hellertown, PA (1973)

9. H. Richter, Proc. of Eleventh International Congress on Glass, Vol. 2, 447, Prague, Czechoslovakia (1977)

Table 1

Table 1. Bulk Density and Open Porosity in SCS-6/Borosilicate Glass Composites

HOT PRESSING TEMPERATURE (^{o}C)	BULK DENSITY (g/cc)	OPEN POROSITY (%)
800	2.151	0.118
700	2.219	0.266
675	2.092	1.677

Figures

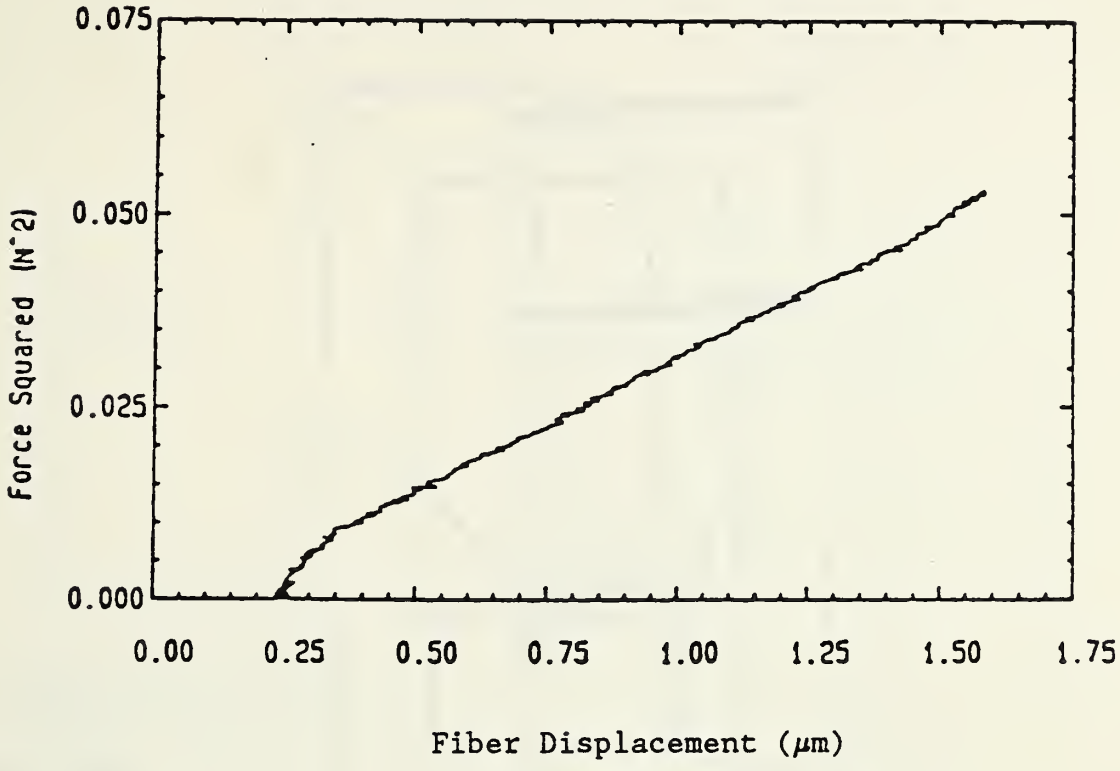

Figure 1. Plot of the square of the force applied to a fiber versus the displacement of the end of the fiber relative to the matrix surface during an instrumented indenter test. The fiber diameter is 17.0 μm.

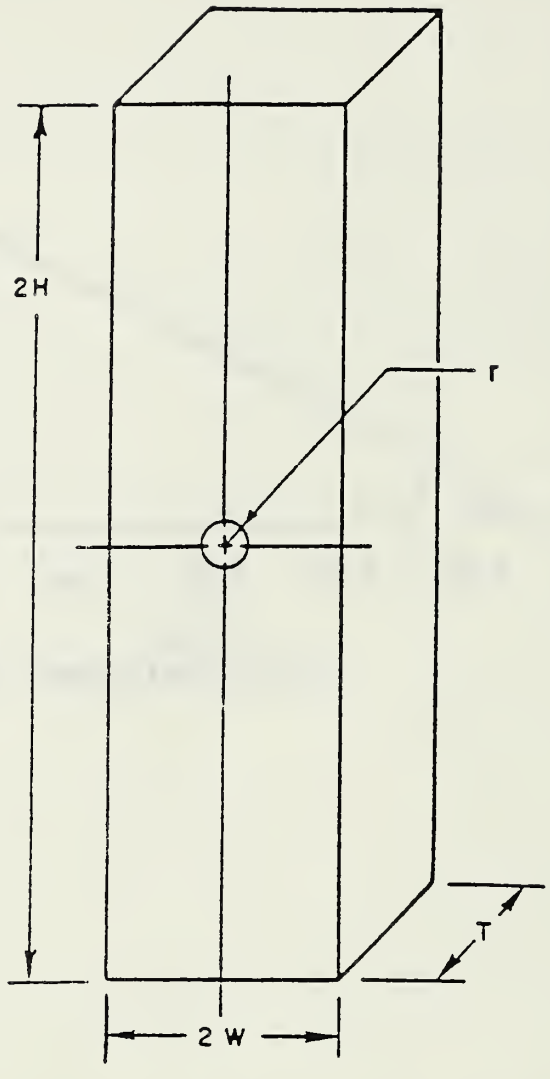

Figure 2. Geometry of a Double Cleavage Drilled Compression (DCDC) Specimen.

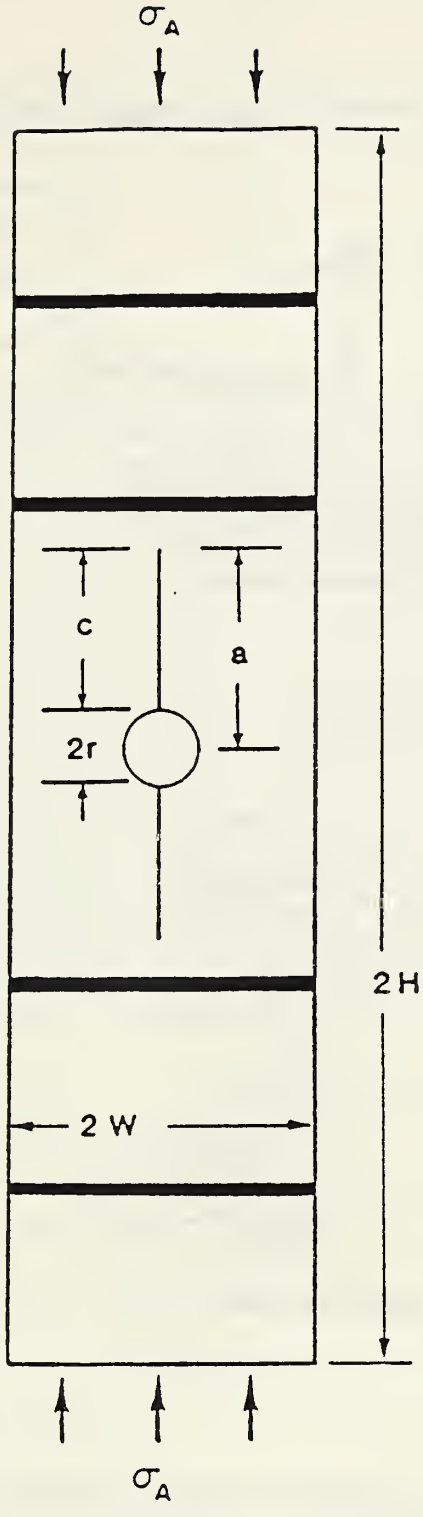

Figure 3. Loaded DCDC specimen with a crack emanating from the top and bottom of the hole.

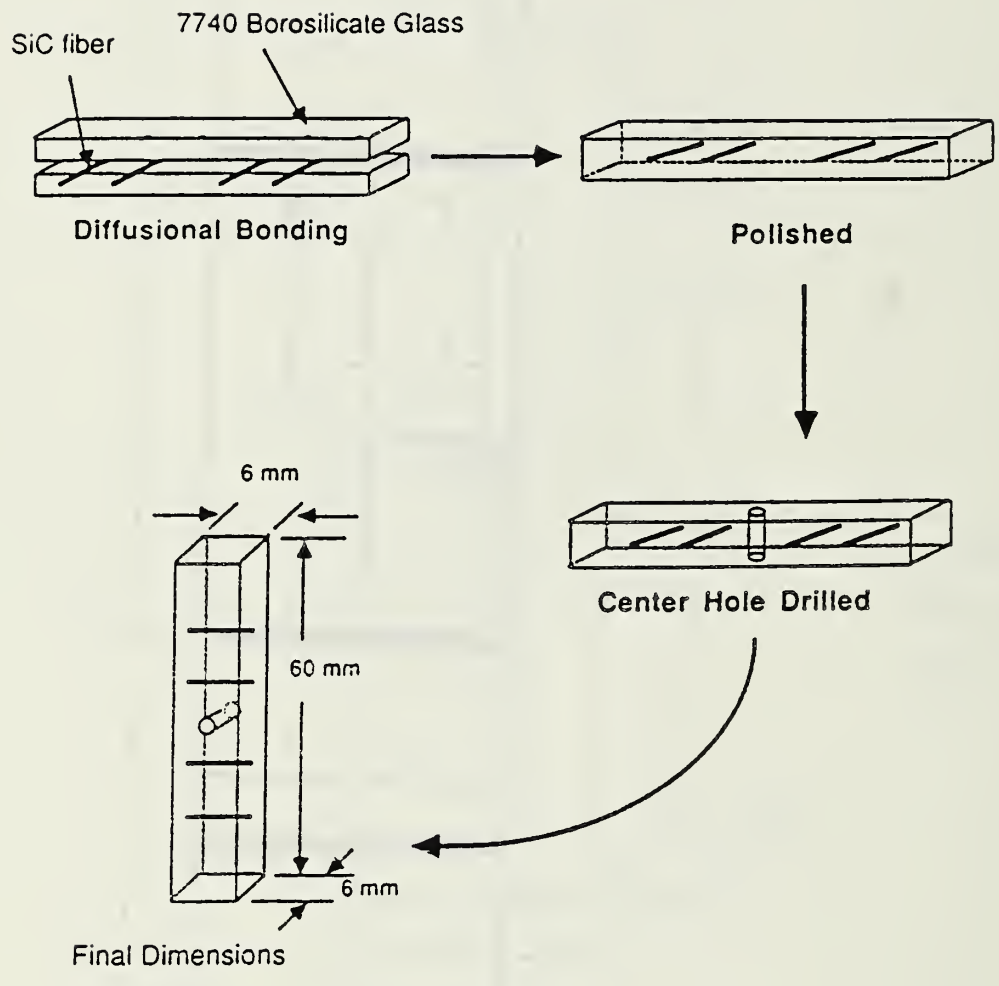

Figure 4. Illustration of the fabrication sequence for the DCDC specimen.

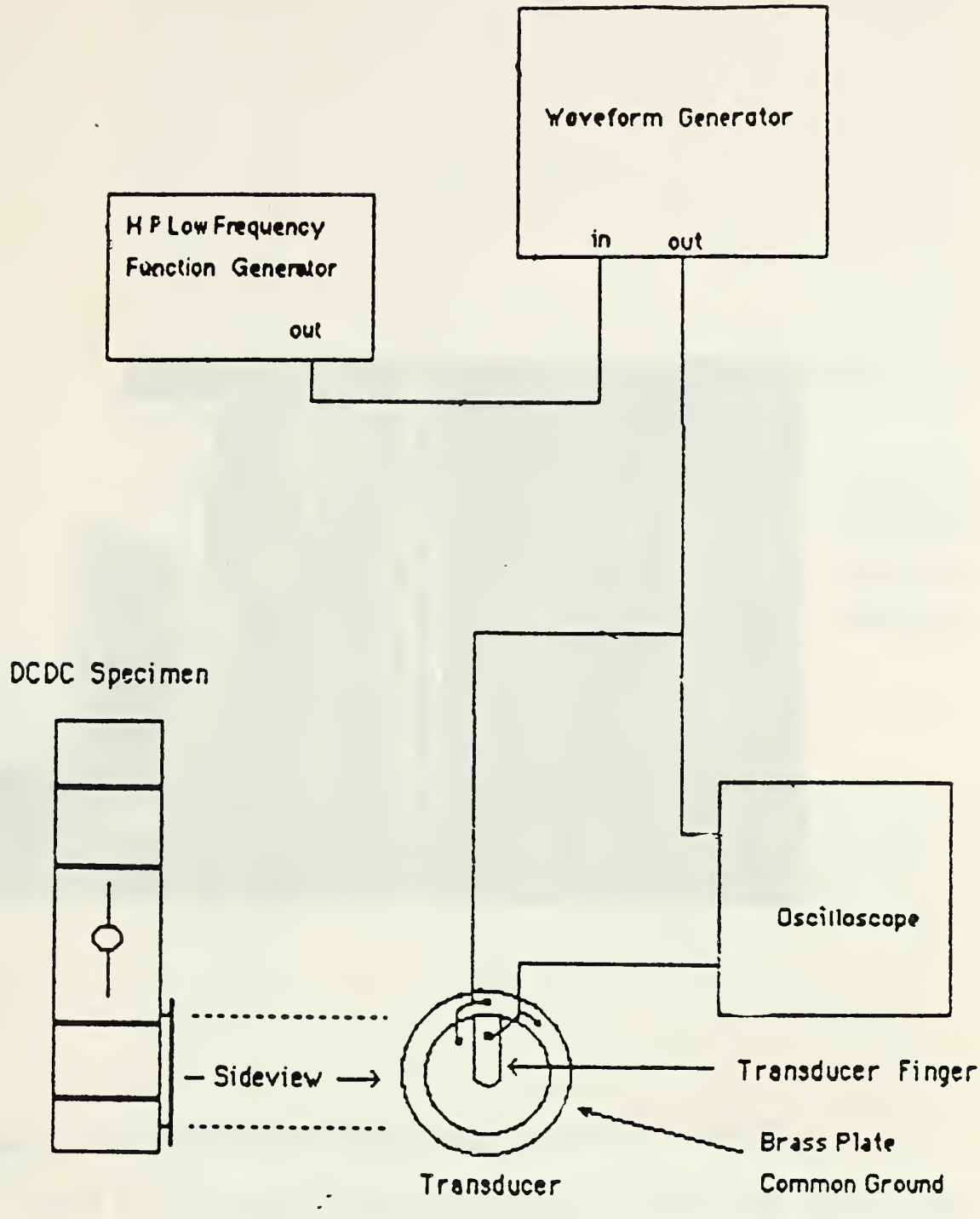

Figure 5. Schematic of Stress-Wave Fractorgraphy Set-up.

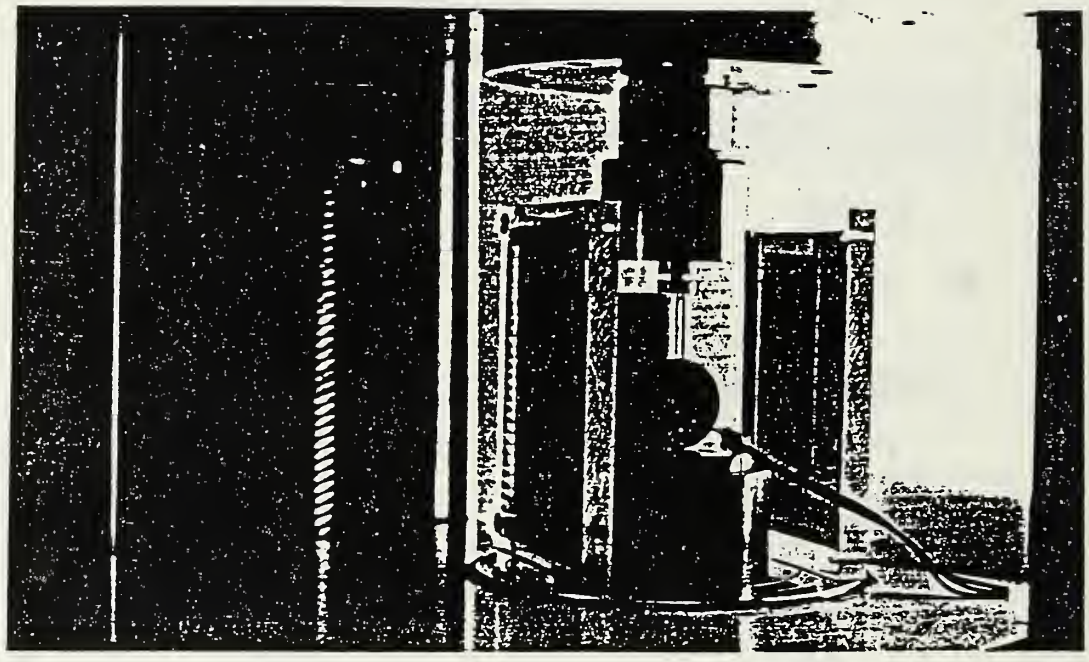

Figure 6. Mechanical testing operation for the DCDC specimen.

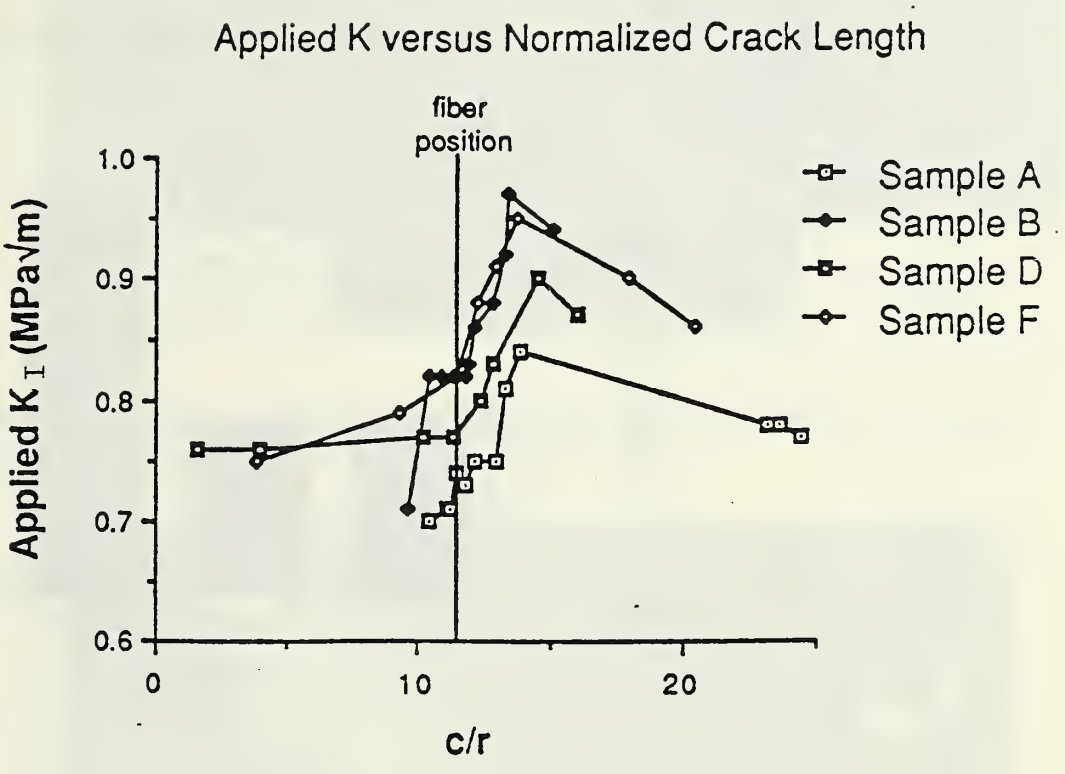

Figure 7. The change in the applied stress intensity with respect to the position of the filament in the DCDC specimen.

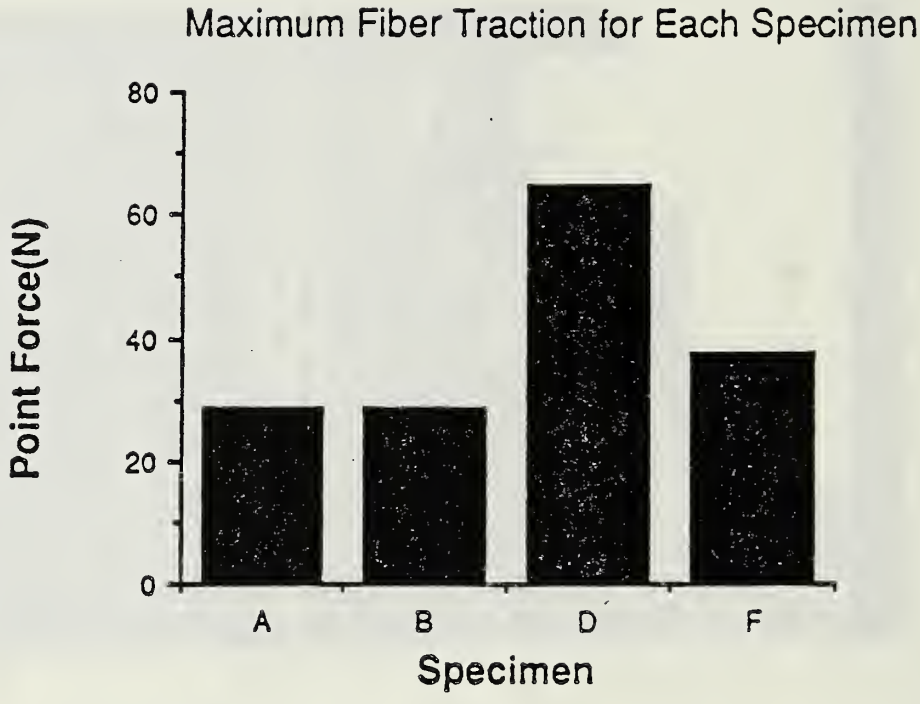

Figure 8. The point force (N) variation from specimen to specimen that i imposed by the fiber at maximum traction as calculated from equation 7.

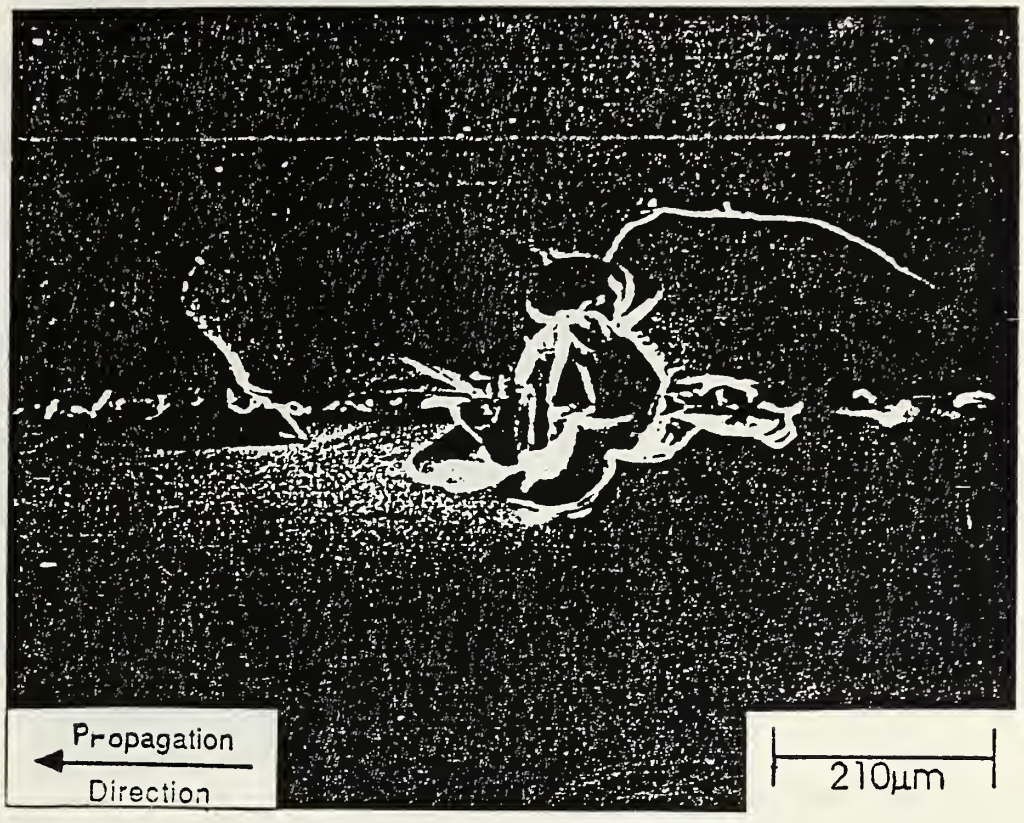

Figure 9. SEM photomicrograph showing a SiC fiber along the fracture surface.

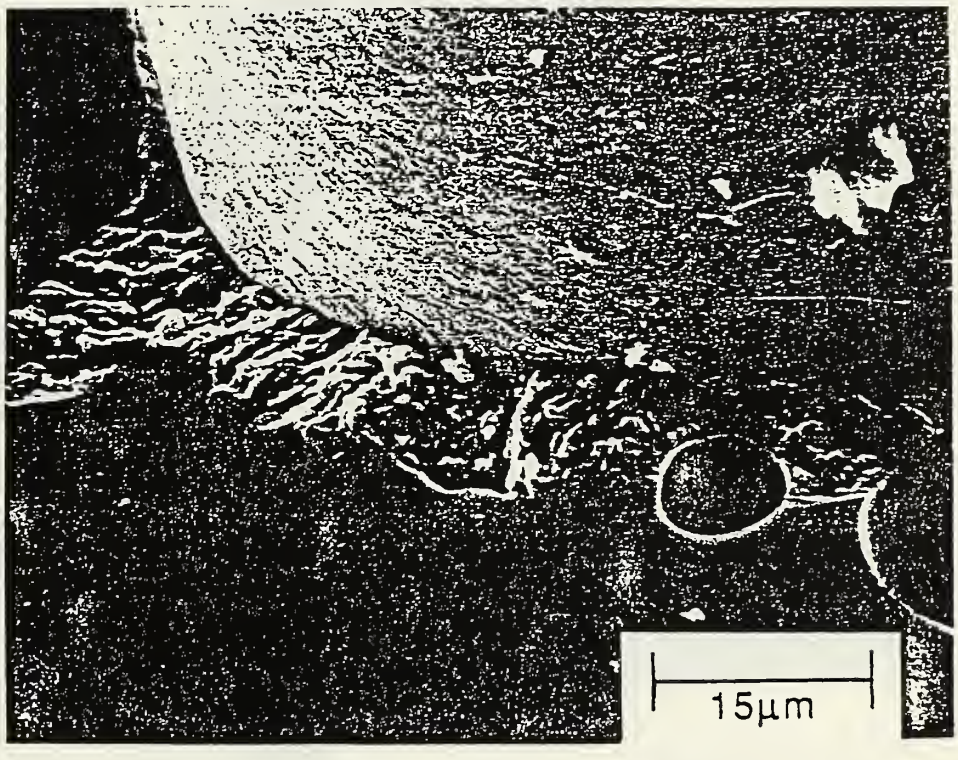

Figure 10. SEM photomicrograph of the alpha-cristobalite layer which forms during fabrication and surrounds the fiber.

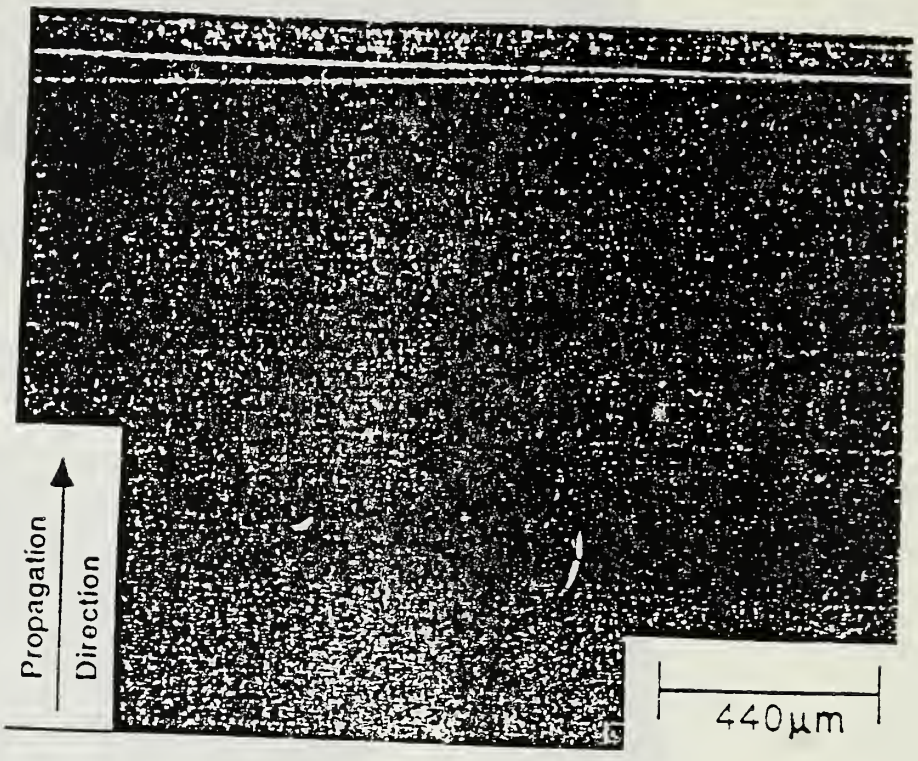

Figure 11. Crack front bowing upon impingement with fiber. (Nomarski polarizing filter in reflected light)

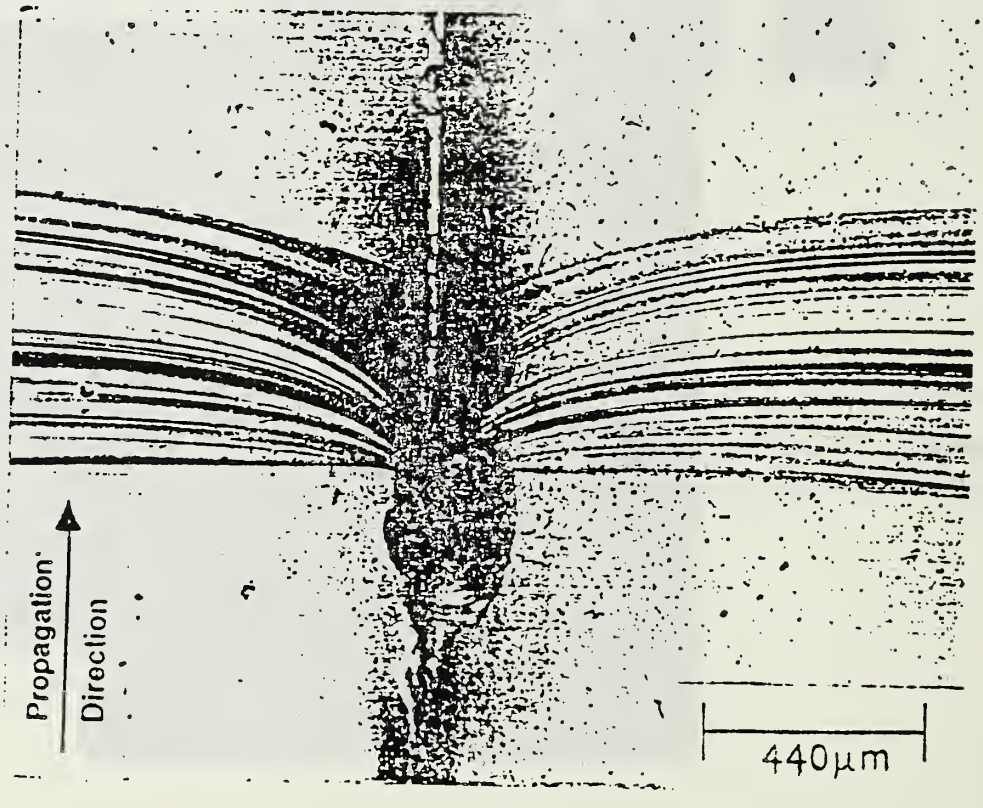

Figure 12. Crack front bowing upon impingement with fiber. (transmitted light)

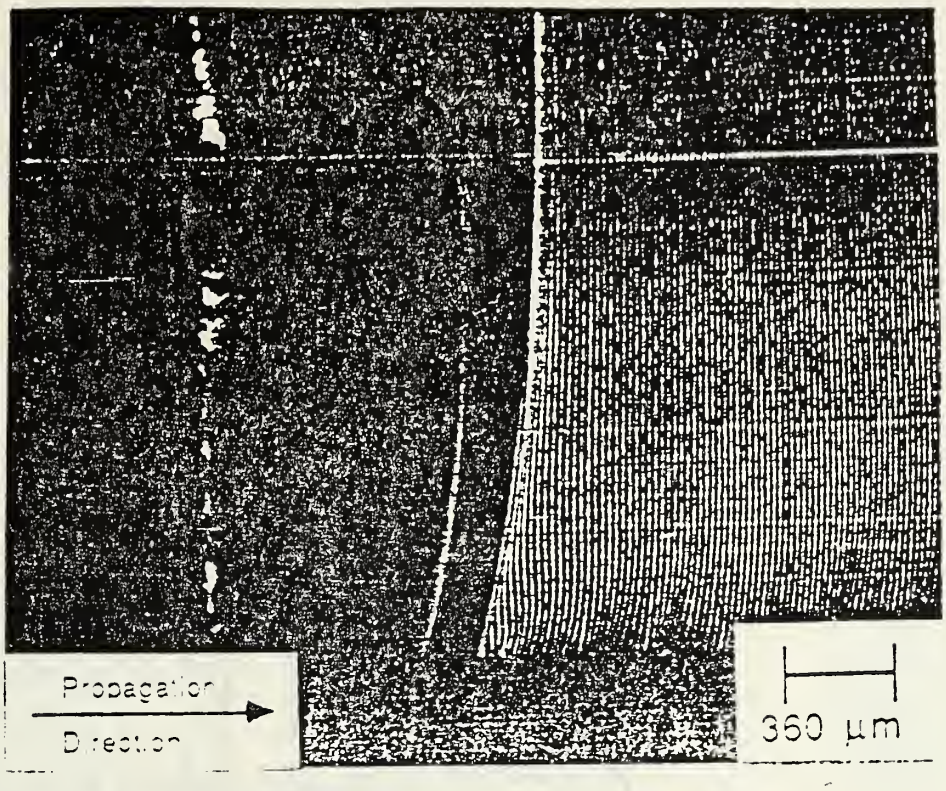

Figure 13. Stress-Wave Photomicrograph, Black region is the center hole. Dark-grey region is the Wallner phenomenon and the vertical undulations follow. Product of a 5 Hz low frequency 80 KHz high frequency gated signal.

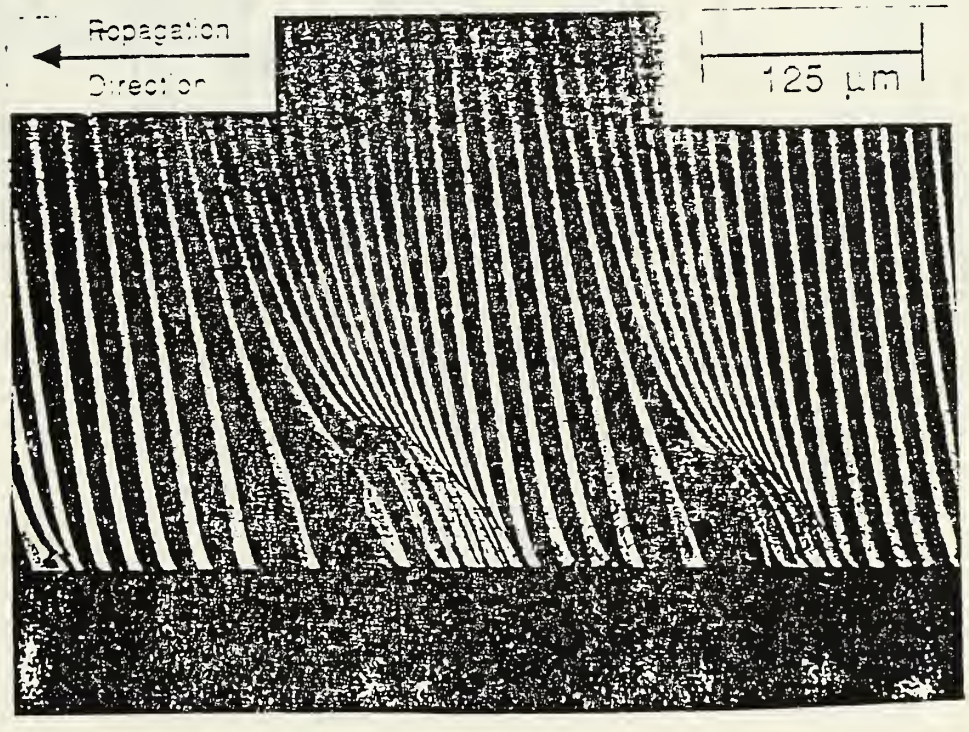

Figure 14. High magnification of the undulation produced with a 5 Hz low frequency, 80 KHz high frequency gated signal along the free edge of the fractured surface.

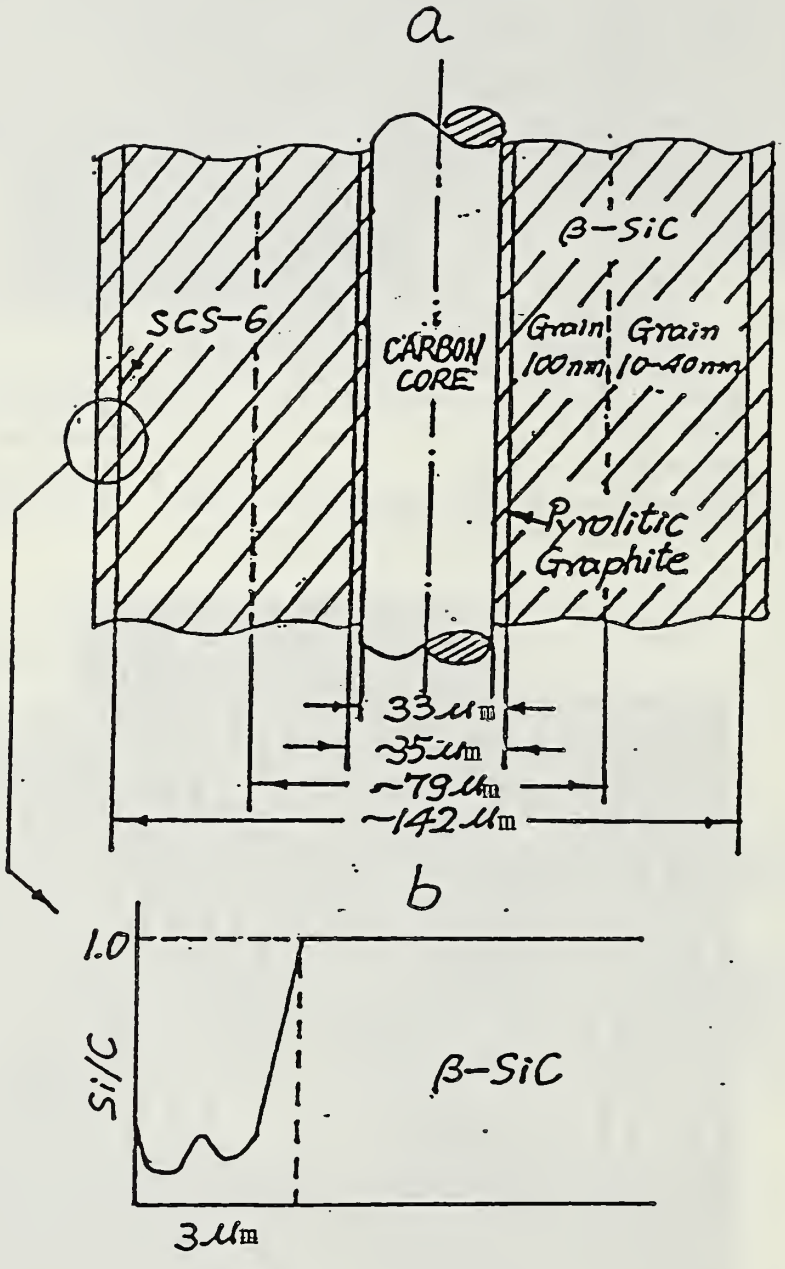

Figure 15 Schematic of a section of AVCO SCS-6 fiber showing various layers and the surface composition.

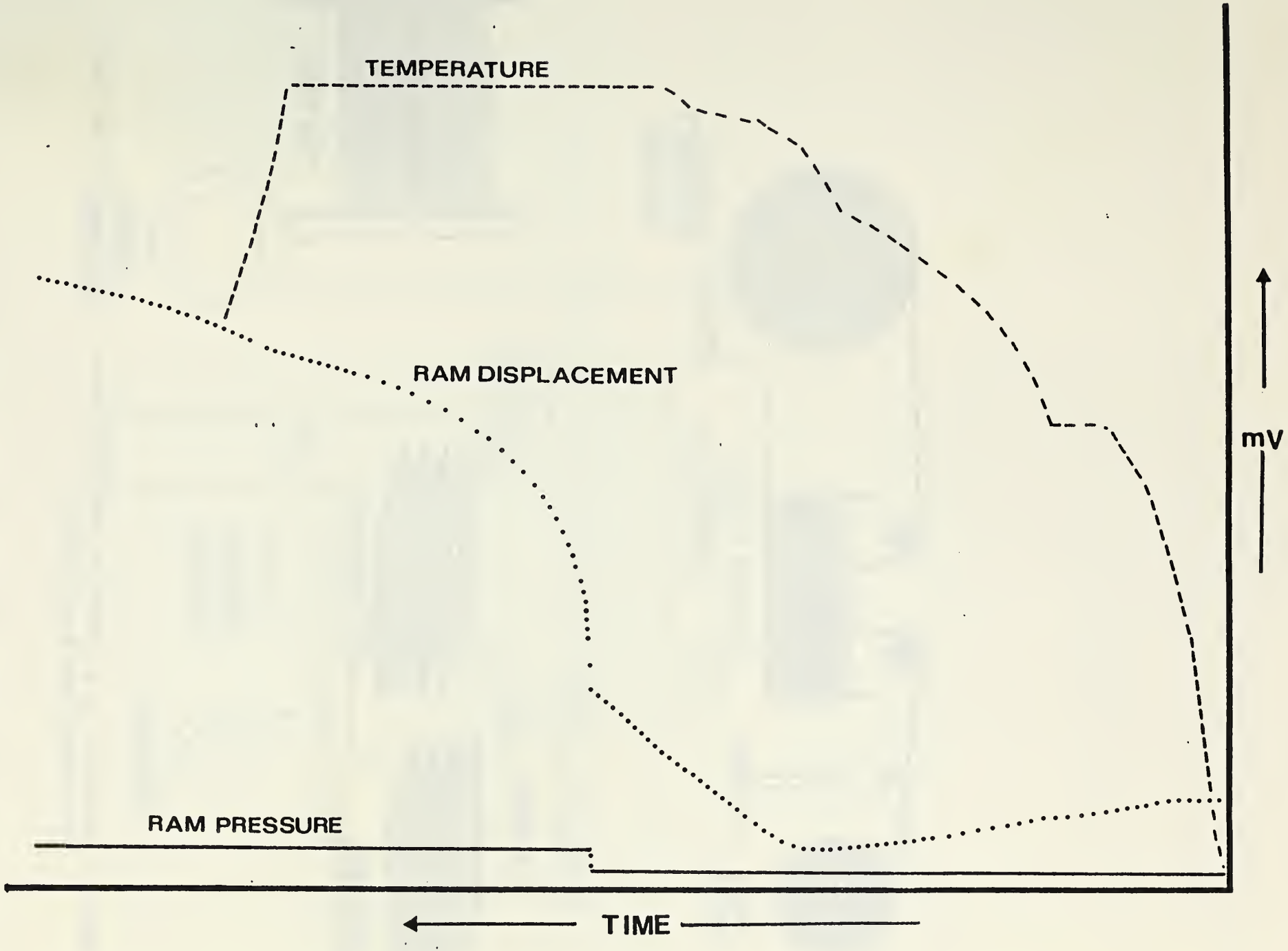

Figure 16 Typical processing parameter chart. Outputs from the various sensing devices such as thermocouple and LVDT are in millivolts. Ram displacement is measured by the LVDT.

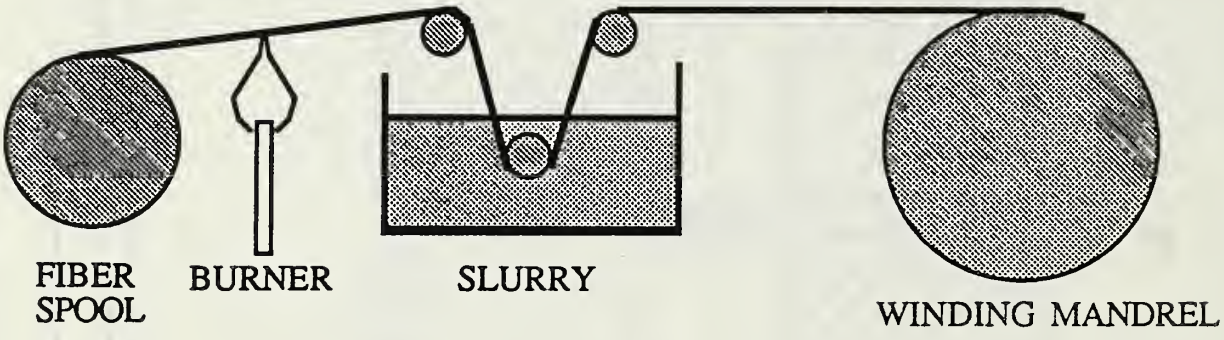

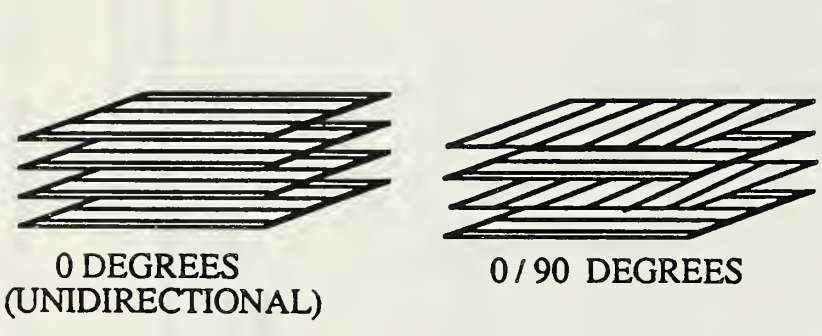

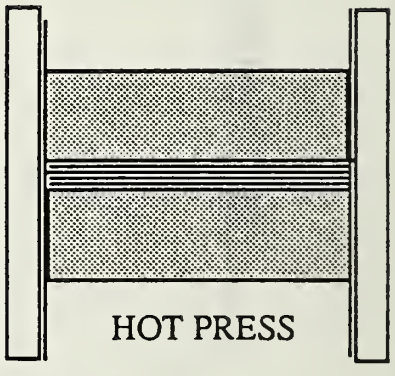

Figure 17 Schematic of a composite making process. After winding the tapes are stacked and hot pressed.

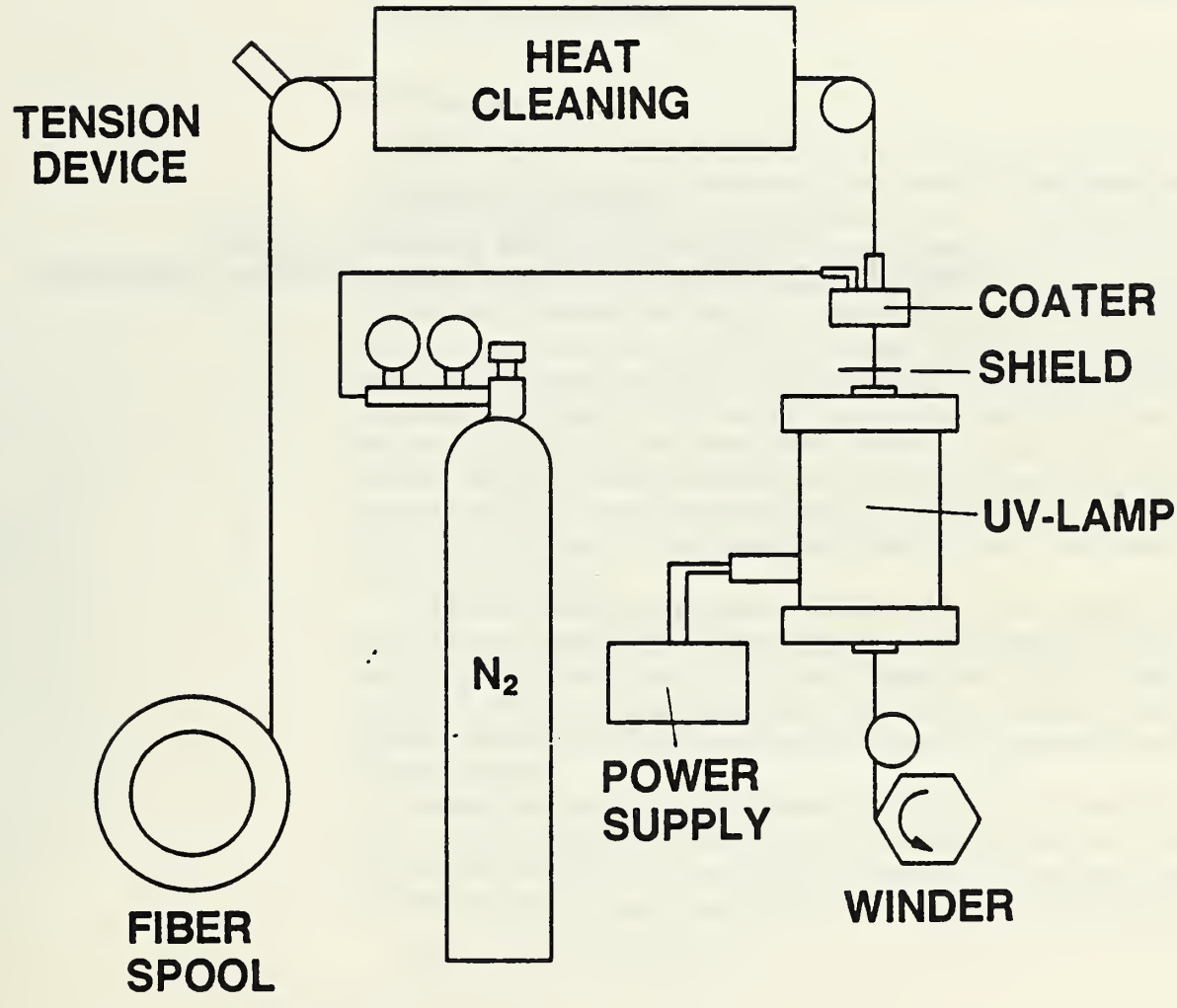

Figure 18 Schematic of polymer coating/UV curing system to coat SCS-6 filaments with glass slurry.

Reprint Entitled
Fracture Mechanics Characterization
Crack/Fiber Interactions in Ceramic Matrix Composites

Reprinted from the Ceramic Engineering and Science Proceedings, Vol. 8, No. 7-8, July-August 1987

Fracture Mechanics Characterization of Crack/Fiber Interactions in Ceramic Matrix Composites

T. W. Coyle, E. R. Fuller, Jr., and P. Swanson

Ceramics Div., Inst. Materials Sci. and Eng.
National Bureau of Standards, Gaithersburg, MD 20899

T. Palamides

Drexel Univ.
Philadelphia, PA

A crucial factor in the structural performance of ceramic matrix composites is the influence of the fiber/matrix bond on the interaction of a matrix crack with the reinforcing fibers. To elucidate the character of this interaction under controlled fracture conditions, glass fracture mechanics specimens were fabricated in the double-cleavage, drilled compression (DCDC) configuration with simple arrays of fibers. Propagating cracks were observed in cross-polarized illumination to characterize delamination of the fiber ahead of the crack and bridging interactions behind the crack tip. Stress wave fractography was employed to analyze the shape and relative velocity of the crack front.

Introduction

A critical issue in the fracture behavior and mechanical performance of ceramic matrix composites is the influence of the strength of the fiber/matrix interface on the interaction of a crack with individual fibers. It is generally accepted that if a strong bond is present between fiber and matrix, cracks run directly through the reinforcing fibers which then have little effect on retarding the propagation of the crack. Although the strength of such a composite may be enhanced through load transfer, the toughness is not appreciably improved and failure is completely brittle. A weak interface leads to crack deflection, debonding along the fiber/matrix interface, and bridging of the crack by the fibers. If the fibers do not break behind the crack tip failure is non-catastrophic. However, if the interface is too weak the fibers slide freely through the matrix and no improvement in strength or toughness is obtained. Thus, a better understanding of the details of this behavior is required before the optimum levels of interfacial strength can be determined for a given fiber-matrix system.

This issue can be investigated experimentally by direct observation of the interaction of a crack with a single fiber in an appropriate fracture mechanics specimen. The double cleavage drilled compression (DCDC) configuration[1] was employed because of the simple shape and loading geometry. No guiding side grooves are required to keep the plane of the crack in the center of this compressively loaded specimen.

Stable crack propagation is obtained in the DCDC specimen since the applied stress intensity (K_{app}) experienced at the crack tip decreases with crack extension at a constant load. From the measured crack length (c) at a given remotely applied compressive stress (σ_{app}), K_{app} can be calculated from the following expression:[1]

$$K_{app}=\sigma_{app}\sqrt{r}/[(c/r)f(c/r)] \quad (1)$$

where the specimen dimensions are as defined in Fig. 1. The function $f(c/r)$ can be determined experimentally by testing specimens of known K_{IC}.

Experimental Procedure

Transparent specimens were produced by sandwiching SiC fibers* between borosilicate glass plates† which were then fused together by heating in air at approximately 850 °C for 10–15 min to produce transparent specimens. The samples were loaded in compression with a screw-driven mechanical testing machine‡ at a crosshead displacement rate of 0.005 cm/min. The strain contours visible in cross-polarized illumination were used to monitor the length of the growing crack and to characterize the crack-fiber interactions.

Stress wave fractography[2] was utilized to monitor the shape of the crack front and the relative velocity of the growing crack along the specimen. Acoustic waves were propagated through the specimen during crack extension by use of a piezoceramic transducer coupled to the specimen. The transducer was driven with bursts of an 80–90 kHz sine wave at a maximum of 30 V peak-to-peak. The burst frequency was 5 Hz; the burst duration was 25% of the low frequency period. This technique produce ripples on the fracture surface at a spacing determined by the frequency of the acoustic excitation. These ripples can then be observed by optical microscopy in reflected light using Nomarsky contrast. With a constant excitation frequency, widely spaced bands indicate a region of rapid crack extension while closely spaced bands indicate relatively slow crack growth.

Results and Discussion

Direct, qualitative observations of several aspects of the fracture behavior in the specimen could be made in transmitted, cross-polarized illumination at various magnifications. Typically the fiber could be seen to bridge the crack for some distance behind the crack tip before breaking. Evidence of localized strain at the fiber-crack surface intersection (Fig. 2) indicated that the bridging fiber was applying tractions across the crack faces. The shape of the strain contours ahead of the crack tip or behind the crack tip away from the crack surfaces gave only occasional faint indications of localized strain which would show load transfer to the fiber. Apparent delamination of the fiber ahead of the crack (Fig. 3) was observed when a higher magnification was used for one specimen.

An optical micrograph of a region of the fracture surface which includes a fiber, taken with Nomarsky contrast, is shown in Fig. 4. The light and dark bands visible under these conditions represent snapshots of the position and shape of the crack front at periodic intervals. It can be seen that the crack front bowed around the fiber which was bridging the crack before the center portion broke away and accelerated to reform a nearly straight front. A scanning electron micrograph of this area (Fig. 5) shows that after bowing around the fiber the two sides of the crack did not meet on the same plane. The resulting ligament would have to have fractured before the center portion of the crack front could extend. From the direct observations discussed above, the fiber appears to have broken at some later time, after the ligament had fractured and the crack front had moved well beyond the fiber. The chipping apparent around the fiber in Fig. 5 would have occurred as the broken fiber was pulled out of the glass matrix.

*SCS-6 Fibers, Avco Corp., Wilmington, MA.
†Corning 7740, Corning Glass Works, Corning, NY.
‡Instron Corp., Canton, MA.

To quantitatively assess the influence of the fibers on the crack propagation the crack length was measured from photographs, such as shown in Fig. 2, and used to calculate the apparent K_{app} from the applied load using Eq. (1). The results for several specimens are shown in Fig. 6. Assuming that the crack is growing at a constant stress intensity, $K_{tip}=K_{IC}$ for the glass matrix, the increase in the calculated K_{app} for crack lengths beyond the fiber position reflects the closure tractions exerted by the bridging fiber (K_{trac}).

$$K_{tip}=K_{IC}=K_{app}=K_{trac} \tag{2}$$

or

$$K_{trac}=K_{IC}-K_{app} \tag{3}$$

The stress intensity factor due to a point force acting at a distance δ behind the crack tip is given by:[3]

$$K_{trac}=-\sqrt{2}\,F/(\pi\delta)^{3/2} \tag{4}$$

where the point force, F, may be a function of δ. Thus, information regarding the forces exerted by the bridging fiber as a function of crack length can be obtained from data such as shown in Fig. 6.

Summary

Sample fabrication methods and experimental techniques have been developed which allow crack-fiber interactions to be directly examined in a ceramic matrix. Qualitative information regarding fiber/matrix debonding, fiber bridging, and pinning and bowing of the crack front at the fiber can be obtained. Possibilities for quantifying the effects of bridging fibers on crack extension in terms of the tractions exerted across the crack by the fiber were demonstrated.

Acknowledgments

Support for this work has been provided by the Department of Energy AR&TD Fossil Energy Materials Program (DE-AI05-800R20679) and by the SDIO/IST program under ONR contract No. N00014-86-F-0096.

References

[1]C. Janssen, "Specimen for Fracture Mechanics Studies on Glass:" pp. 23-30 in Proceedings of the Xth International Congress on Glass, Kyoto, Japan, July 8-13, 1974. The Ceramic Society of Japan, Kyoto, Japan.

[2]H. Richter, "Crack Propagation in Glass Under Liquids in an Intermediate Range of Crack Velocities:" pp. 219-29 in Strength of Inorganic Glass, Ed. by C. R. Kurkjian, Plenum Publishing Corp., 1985.

[3]H. Tada, P. C. Paris, and G. R. Irwin, The Stress Analysis of Cracks Handbook, Del Research Corp., Hellertown, PA., 1973.

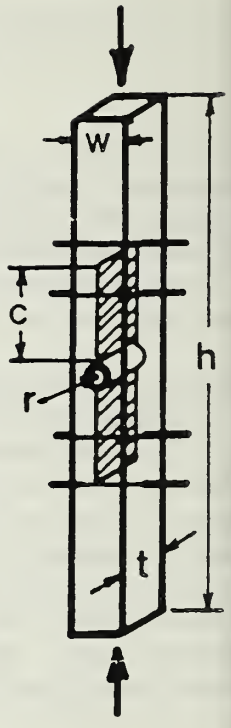

Fig. 1. Double-cleavage drilled-compression fracture mechanics specimen. Compressive load opens cracks above and below centered hole.

Fig. 2. View perpendicular to fiber axes of DCDC specimen under load. The cracks are seen edge-on with the crack tips located between the inner and outer fibers. Strain contours are visible by virtue of the transmitted cross-polarized illumination.

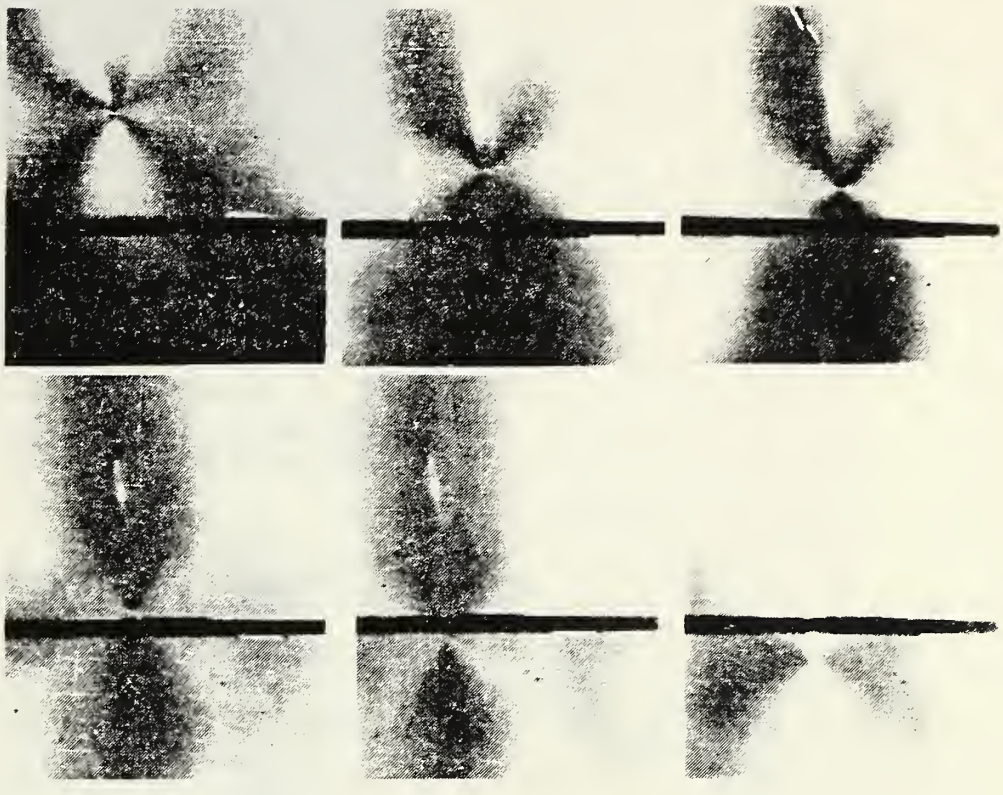

Fig. 3. Higher magnification views in cross-polarized transmitted light of region near reinforcing fiber. Crack-tip is seen approaching and then passing the fiber as the remotely applied load is increased. Field of view is approximately 2.7 mm wide.

Fig. 4. Optical micrograph of a region of the fracture surface centered about a reinforcing fiber. Nomarsky contrast reveals the periodic surface undulations caused by the applied acoustic waves. The crack was propagating from right to left. The field of view is approximately 1 mm wide.

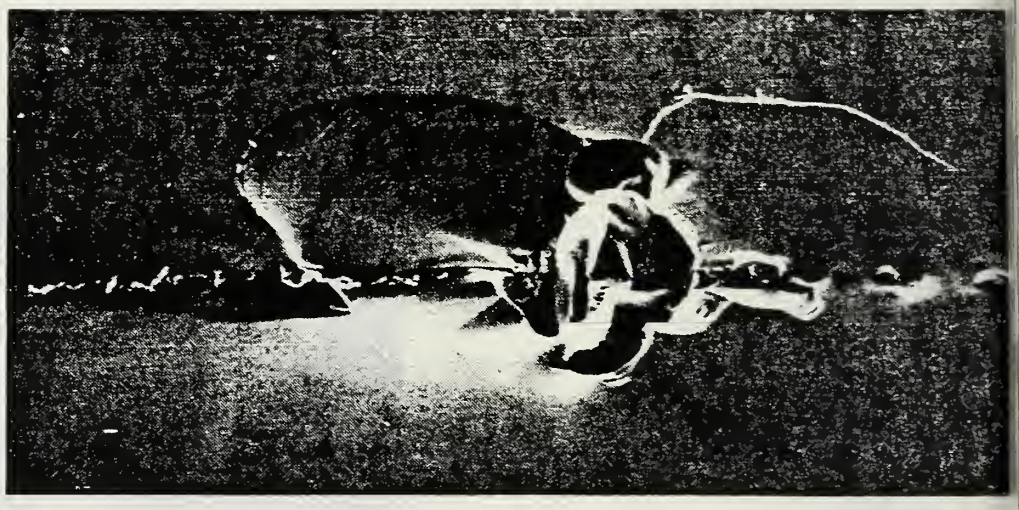

Fig. 5. Scanning electron micrograph of area shown in Fig. 4. The remnant of the ligament formed as the crack front swept around the fiber can be seen to the left of the fiber. (Field of view approximately 1.1 mm wide.)

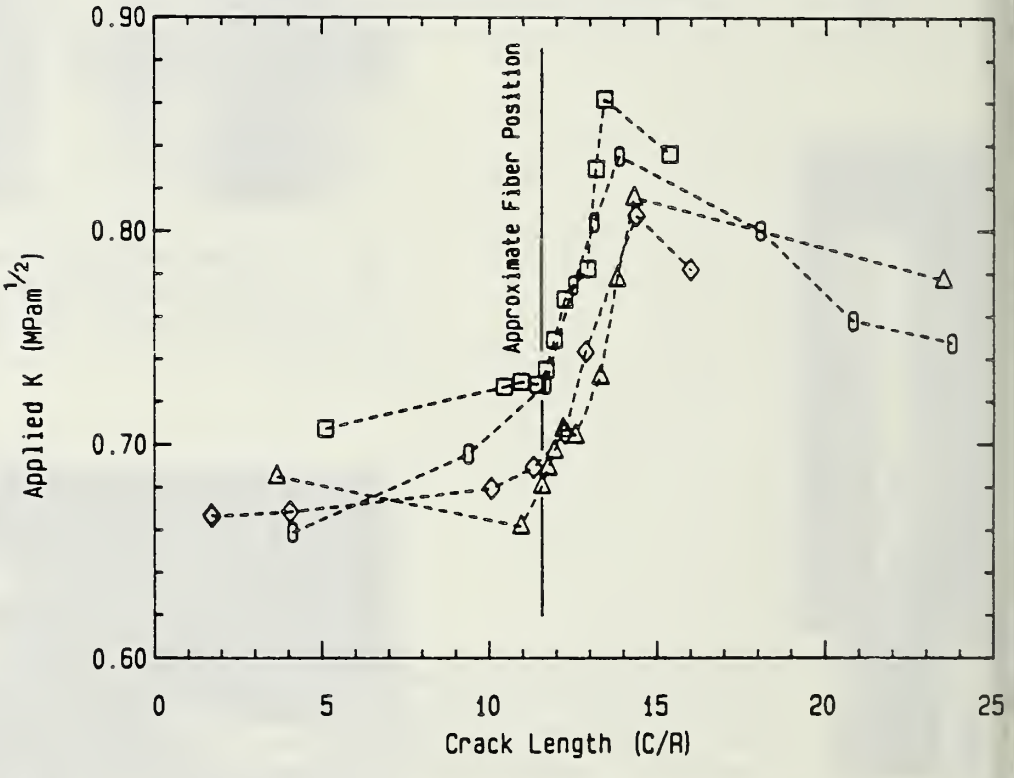

Fig. 6. Plot of remotely applied K (calculated from Eq. (1)) vs crack length showing relative position of the reinforcing fiber. Increase in the applied K required to propagate the crack reflects the closure forces exerted by the bridging fiber.

Proceedings of the 1987 Northeast

Regional ASM Meeting

CRACK-FIBER INTERACTIONS IN CERAMIC MATRIX COMPOSITES

T. W. Coyle, T. R. Palamides*, S. W. Freiman,
E. R. Fuller and U. V. Deshmukh*

Ceramics Division
Institute for Materials Science and Engineering
National Bureau of Standards
Gaithersburg, MD

*Drexel University
Philadelphia, PA

Abstract

Crack-fiber interactions are the key to the unique properties of continuous fiber reinforced ceramic matrix composites. This paper describes the development of a fracture mechanics technique for examining crack-fiber interactions in model SiC fiber reinforced glass specimens. Direct examination of the closure force imposed by a bridging fiber on a crack was accomplished using the double-cleavage drilled-compression sample. The stress intensity at the crack tip is described in terms of the applied load and the closure force. The closure force is a function of the interfacial bonding and/or frictional forces between the fiber and the matrix. Evaluation of these interfacial forces by indentation experiments in which the indentation load and the displacement of the fiber are measured directly is described.

Introduction

The fracture behavior of brittle matrix/brittle fiber composite systems is strongly dependent on the mechanical performance of the fiber/matrix interface. For a given set of fiber and matrix properties, the fracture characteristics can range from the desired fibrous, non-catastrophic failure to a completely brittle, low toughness fracture, depending on the interfacial properties. The first condition which must be met to avoid a completely brittle failure mode is for the interface to be weak enough to allow debonding to occur between the fiber and matrix ahead of the crack tip or to cause the matrix crack to deflect along the interface. Fracture mechanics treatments of cracks at bi-material interfaces[1,2] provide some guidance regarding the relative strength levels required among matrix, fiber, and interface to achieve the desired interfacial failure but direct experimental studies are lacking.

When the interface has debonded, the fiber can remain bridging between the crack faces after the matrix crack has advanced. Propagation of the matrix crack is then opposed by the closure forces exerted on the crack by the bridging fibers. The nature of these closure forces is controlled by the shear properties of the interface and the fiber modulus and strength. Recent modelling of this situation by Marshall, Evans and coworkers[3,4] indicates that the bridging fibers can either remain intact behind the crack tip leading to non-catastrophic failure or can break at some distance behind the crack tip resulting in a failure which is primarily brittle in nature, although with a higher toughness than the unreinforced matrix. Experimental results suggest that the trends predicted by the model with changes in interfacial character are correct, but detailed studies over the range of possible behavior are not yet available.

Direct experimental examination of the interactions between matrix cracks and reinforcing fibers is therefore valuable in furthering the understanding of the influence of interfacial properties on fracture behavior. Develop of techniques to investigate these issues are described in the following along with observations on a model ceramic matrix system, SiC fiber reinforced glass. The double cleavage drilled compression (DCDC) configuration[5] was used to study the effects of individual SiC fibers on crack propagation in glass specimens. Qualitative observations of the shape of the crack front and the fracture path in the vicinity of the fiber were made and some quantitative information regarding the closure forces exerted by bridging fiber was obtained. The fiber/matrix interfacial shear properties were evaluated independently by measuring the force required to push the fibers through thin sections of the glass matrix using an indentation technique. The results of these tests are discussed in terms of the current views of fracture in ceramic matrix composites.

Experimental Procedure

Transparent DCDC specimens were produced by sandwiching SiC fibers* between borosilicate glass plates# which were then fused together by heating in air at approximately 850°C for 20 to 30 minutes. The samples were ground to size using standard diamond machining techniques. The four sides were then polished with the final surface finish produced by 0.05μm Al_2O_3 powder. The dimensions, as defined in Fig. 1, were nominally t = w = 6mm and

---

* SCS-6 Fibers, Avco Corp., Wilmington, MA.

h = 60mm, with a hole radius of 0.8mm. The fibers were placed symmetrically about the central hole with the inner fibers located approximately 9mm from the hole. The specimens were loaded in compression using a screw-driven mechanical testing machine* at a cross-head displacement rate of 0.05 mm/min.

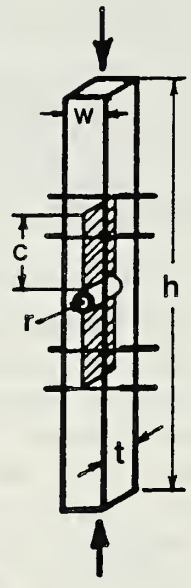

Figure 1 - Double-cleavage drilled-compression fracture mechanics specimen. Compressive load opens cracks above and below centered hole.

Transmitted cross-polarized illumination was used perpendicular to the fiber axis to produce visible strain contours in the specimens. The contours enabled the uniformity of the applied loading to be evaluated, the crack length to be determined, and local strain concentrations associated with the crack-fiber interactions to be detected.

The shape of the crack front and the relative velocity of the growing crack along the specimen were monitored by stress wave fractography.[6] Acoustic waves were propagated through the specimen during crack extension by use of a piezoceramic transducer coupled to the specimen through silicon grease. The acoustic waves produce ripples on the fracture surface which can be observed by optical microscopy in reflected light using differential interference contrast. Each "ripple" marks the position of the crack front at periodic intervals set by the excitation frequency of the transducer, therefore the spacing of the ripples is a measure of the local crack velocity. The transducer was driven with bursts of an 80-90 KHz sine wave at a maximum amplitude of 30 V peak to peak. The burst frequency was 5 Hz; the burst duration was 25% of the low frequency period.

To characterize the mechanical behavior of the fiber/matrix interface in shear, the fibers were pushed through thin sections of the matrix by applying an axial load on the fiber using a Vicker's hardness machine. The hardness tester was instrumented to allow the applied load and the displacement of the diamond indenter to be measured continuously during the testing cycle. Samples were prepared from the broken halves of the DCDC specimens by diamond grinding them to a thickness of approximately 0.85mm perpendicular to the fiber axis and then polishing.

Results and Discussion

A view of a DCDC specimen under load in cross-polarized transmitted light which illustrates the type of qualitative observations that could be made is shown in Fig. 2. The strain contours are symmetric about the center line of the specimen indicating that the specimen is well aligned. The crack emanating from the central hole is seen edge-on with the crack tip located at the center of the hour-glass shaped pattern formed by the strain contours. At this point in the test the crack tip has already moved past the first fiber and is now between the inner and outer fibers. A change in contrast indicating a region of localized strain could be observed in the area where the fiber intersects the crack, demonstrating that the fiber was bridging the crack and exerting a closure force across the crack faces. This feature disappeared following further crack growth, suggesting that the fiber broke at some distance behind the crack tip.

Figure 2 - View perpendicular to fiber axes of DCDC specimen under load. Strain contours are visible by virtue of the transmitted cross-polarized illumination.

An optical micrograph of a fracture surface in the region about the inner fiber, taken with differential interference contrast, is shown in Fig. 3. The fiber axis is perpendicular to the plane of the photograph. The light and dark bands visible under these imaging conditions represent "snapshots" of the position and shape of the crack front at periodic intervals. With a constant excitation frequency applied to the piezoceramic transducer, closely spaced bands indicate slow crack growth, while widely spaced bands reflect regions of more rapid crack propagation. It can be seen that the crack front bowed around the fiber which was bridging the crack before the center portion broke away and accelerated to reform a more nearly straight front. A scanning electron micrograph of the same area (Fig. 4) shows that after bowing around the fiber the two sides of the crack did not meet on the same plane. Fracture of the ligament which formed between the two crack planes was necessary before a continuous crack-front could reform. The scallop-shaped chips around the fiber occurred during fiber pullout. From the indications of bridging which could still be observed in transmitted polarized illumination after the crack had propagated well beyond the fiber,

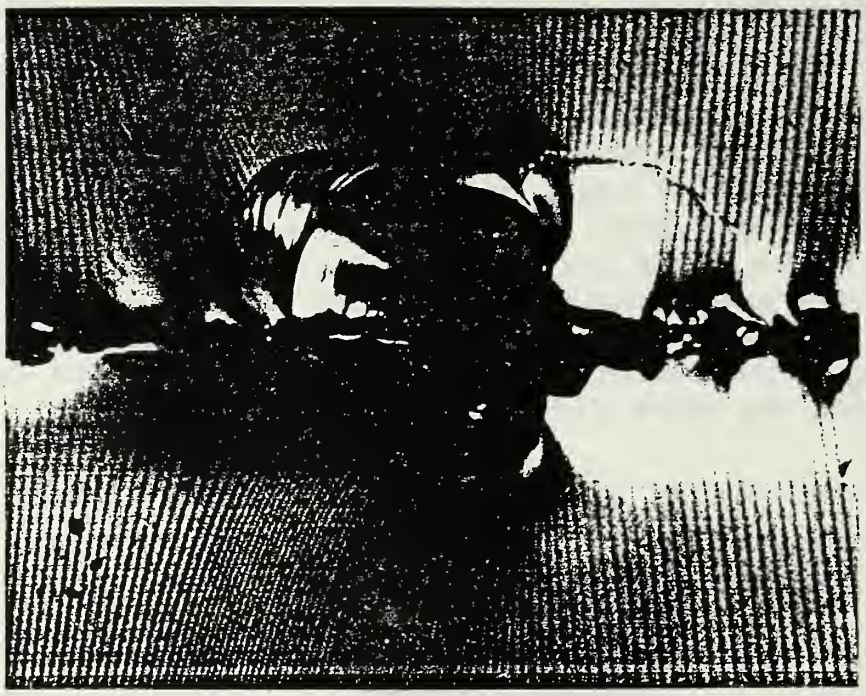

Figure 3 - Optical micrograph of a region of the fracture surface centered about a reinforcing fiber. Differential interference contrast reveals the periodic surface undulations caused by the applied acoustic waves.

Figure 4 - Scanning electron micrograph of area shown in Fig. 6. The remnant of the glass ligament formed as the crack swept around the fiber can be seen to the left of the fiber.

The quantitative information obtained from the tests is based on stress intensity factor analyses of the DCDC specimen[5-9] which indicate that for a wide range of crack lengths the stress intensity factor (K_{app}) due to the remotely applied compressive load (σ_{app}) is well described as a linearly decreasing function of crack length (c). The expression

$$\frac{\sigma_{app}\sqrt{r}}{K_{app}} = \alpha \frac{c}{r} + \beta \qquad (1)$$

where r is the radius of the center hole in the DCDC specimen, was used to calculate K_{app} from the applied load and crack lengths measured from photographs such as shown in Fig. 2. The constants α and β were evaluated empirically by testing specimens of known K_{IC}. In Fig. 5 the calculated K_{app}, with α=0.151 and β=2.158, is plotted versus c/r for several specimens. Assuming that the crack is growing at a constant stress intensity, $K_{tip} = K_{IC}$ for the glass matrix (0.77 $MPam^{1/2}$)[5], the increase in the calculated K_{app} for crack lengths beyond the fiber position reflects the contribution to the total stress intensity of the closure force exerted by the bridging fiber (K_{fib}):

$$K_{tip} = K_{IC} = K_{app} + K_{fib} \qquad (2)$$

or

$$K_{app} = K_{IC} - K_{fib} \qquad (3)$$

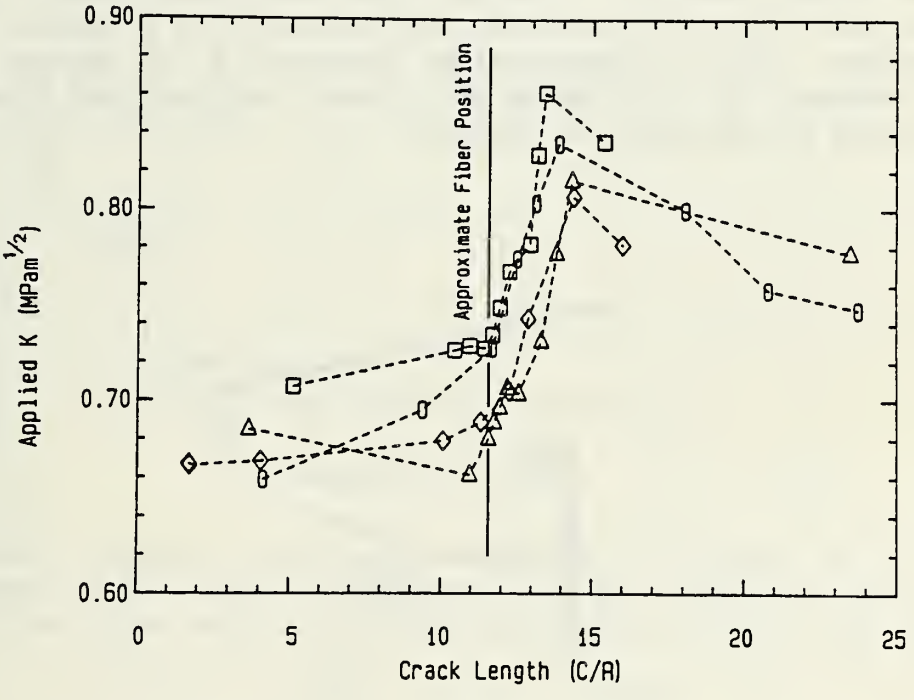

Figure 5 - Plot of applied K due to remotely applied compressive load versus crack length showing relative position of the reinforcing fiber.

The measured crack lengths used to construct Fig. 5 are through thickness averages of the crack length along the crack front. In unreinforced specimens such measurements are adequate since the crack front is nearly straight. However, as seen in Fig. 3 the crack front is curved in the region near the fiber, therefore analysis of these results should incorporate this feature. Assume that the crack front assumes a profile such

curvature must arise from the form of the expression for K_{fib}. The stress intensity factor along a straight crack front due to a point closure force, F, acting at a distance, x, behind the crack tip is given by[10]:

$$K_I = - \frac{\sqrt{2}\ F}{(\pi\ x)^{3/2}} \left(\frac{x^2}{x^2 + z^2} \right) \tag{4}$$

where z describes the position along the crack front (Fig. 6). Substitution of Eq. 4 for K_{fib}, with F taken as the bridging force due to the fiber, and Eq. 1 for K_{app} in Eq. 2 results in an expression which describes contours in the x-z plane (the fracture surface) where $K_{tip} = K_{IC}$ for given values of σ_{app} and F,

$$K_{tip} = \frac{\sigma_{app}\sqrt{r}}{\alpha\frac{x}{r} + \alpha\frac{a}{r} + \beta} - \left(\frac{\sqrt{2}\ \sqrt{x}\ F}{\pi^{3/2}\ (x^2 + z^2)} \right) \tag{5}$$

where a is the distance from the edge of the center hole to the fiber. It is difficult at this time to estimate the error involved in applying Eq. 4 to a curved crack front. Near the fiber, where the crack front curvature is large, Eq. 4 may overestimate K_{fib} by as much as a factor of two or three. The approximation of F as a point force also becomes inadequate within a few fiber radii of the fiber location. Farther from the fiber, where the change in x becomes small with respect to z along the contours of constant K_{tip}, the error should be modest. With an appropriate value of F, it should therefore be possible to account for the observed crack lengths and crack front profiles as a function of the applied stress.

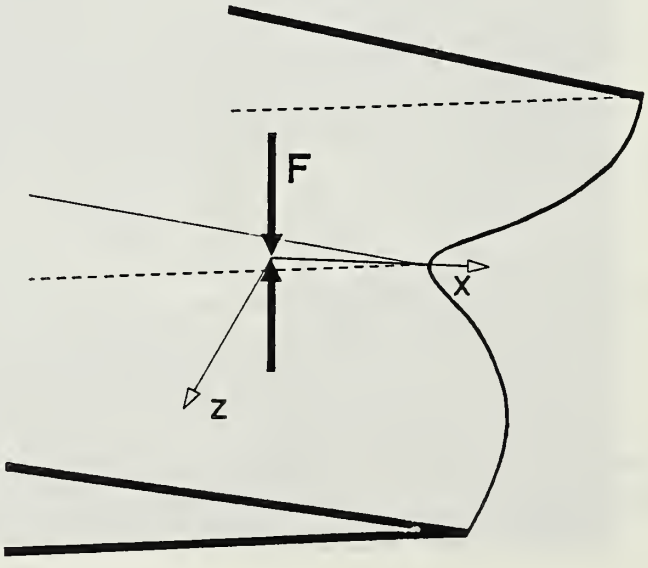

Figure 6 - Schematic illustration of the bowed crack-front profile showing the x-z coordinate system defined on the fracture surface with origin located at the position of the closure force, F.

The closure force is transferred from the fiber to the matrix through shear tractions acting across the fiber/matrix interface. Therefore the closure force exerted across the crack surfaces is controlled by the interfacial properties. To independently evaluate the response of the interface to applied shear stresses an instrumented hardness machine was used to push the fibers through thin sections fabricated from the broken halves of the DCDC specimens. Measured load-displacement curves for two fibers are shown in Fig. 7. The load-displacement records for these tests typically showed a maximum in the applied load followed by an abrupt drop to a plateau load nearly constant over several micrometers of displacement. The increase in load beyond the plateau results from the indenter making contact with the matrix surrounding the fiber. The customary interpretation of this type of result is that the peak applied load corresponds to the applied shear stress required for debonding (τ_{db}) and the plateau load to the stress for frictional sliding (τ_f). Observed values of τ_{db} ranged from 0.8 to 1.0 MPa and of τ_f from 0.4 to 0.7 MPa. An estimate of the magnitude of F is obtained by multiplying τ by the interfacial area, i.e. $F = (\pi\ D\ w/2)\ \tau$.

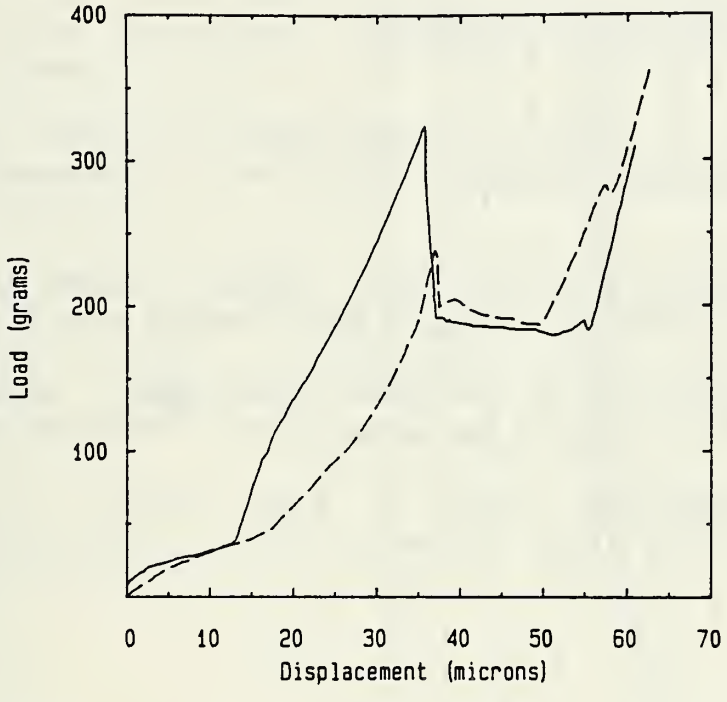

Figure 7 - Curves showing axial load applied to the end of a fiber by the Vicker's indenter versus the displacement of the indenter. The abrupt load drop occurs as the fiber begins to slide through the glass matrix.

Contours of $K_{tip} = K_{IC}$ given by Eq. 5 with F = 0.7N for several levels of applied stress are shown in Fig. 8, where the point force is located at the origin. The shape of the calculated constant K_{tip} contours have the same general shape as the crack front profiles shown in Fig. 3, suggesting that the character of the bridging interaction is fairly well described by Eq. 4. The spatial extent of the calculated interaction is also in fair agreement with that observed, indicating that the magnitude of the trial bridging force is of the correct order. However, in the region near the fiber, where the interactions are strongest, the calculated contours do not describe the experimental observations very well. This may be due to the assumption of

From the results of the indentation experiments it is clear that the force exerted by the fiber varies with the relative displacement of the fiber and the matrix. The bridging force will therefore depend on the debonded length and the crack opening displacement (u). In principle the dependence on crack opening displacement could be introduced into Eq. 4 by taking $F = f(x)$. For example, when a simple frictional sliding resistance (τ_f = constant) can be used to describe the resistance to shear of the interface, F increases with $\sqrt{u}$ (i.e. $F \propto (u^{1/2}))^{3,4}$. Assuming $u \propto (x^{1/2})$ would then give $F \propto (x^{1/4})$. Substitution of such an expression for F in Eq. 6 may yield better agreement with the observed crack front contours. However, several other factors influence the shape of the contours in the region near the fiber. The importance of debonding relative to frictional slippage, the debonded or slippage length, and the errors involved in applying Eq. 4 to this situation can also affect the agreement between the calculated and observed contours. The work now in progress is concentrated on assessing the relative importance of these factors.

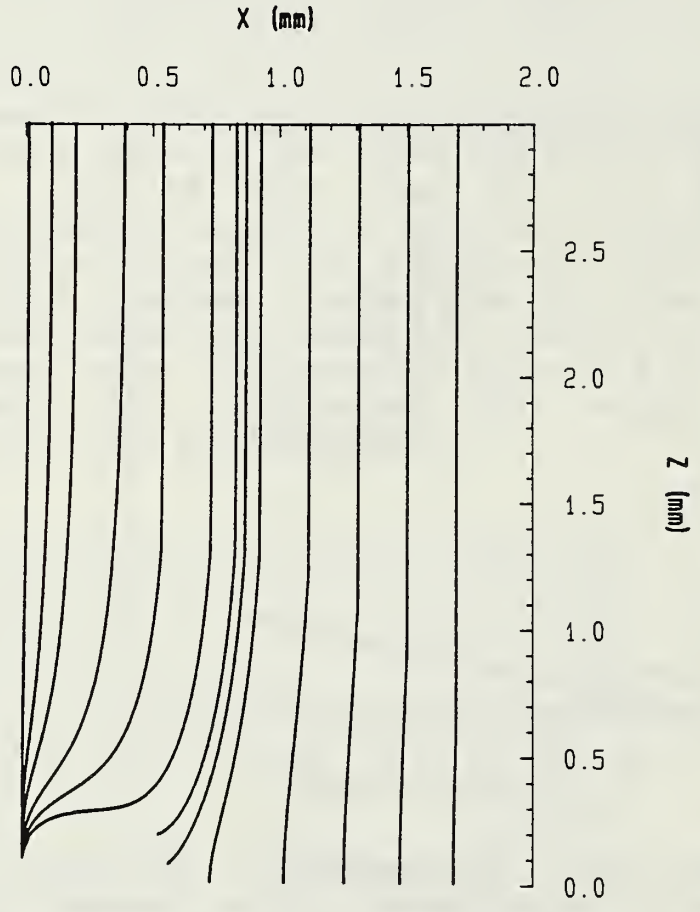

Figure 8 - Contours of constant K_{tip} on the x-z plane (the fracture surface) calculated using Eq. 5 for several values of σ_{app} with F = 0.7N. Each contour, from left to right, corresponds to a larger σ_{app}. The point force (the fiber) is located in the lower left corner (x = 0, z = 0). The area represented would extend from the center line of the DCDC specimen at z = 0 to the specimen edge at z = 3.0.

References

1. T. S. Cook and F. Erdogan, "Stresses in Bonded Materials with a Crack Perpendicular to the Interface", Int. J. Engng. Sci., 10 (1972) 677.

2. J. R. Rice and G. C. Sih, "Plane Problems of Cracks in Dissimilar Media", J. Appl. Mech., 32 (1965) 418.

3. D. B. Marshall, B. N. Cox, and A. G. Evans, "The Mechanics of Matrix Cracking in Brittle-Matrix fiber Composites", Acta Metall., 33 (1985) 2013-2021.

4. D. B. Marshall and A. G. Evans, "Tensile Failure of Brittle-Matrix Fiber Composites", Proceedings of the 5th International Conference on Composite Materials, ICCM-V, ed. W. C. Harrigan, J. Strife, and A. K. Dhingra (Warrendale, PA: The Metallurgical Society, 1985), 557-568.

5. C. Janssen, "Specimen for Fracture Mechanics Studies on Glass", Proceedings of the Xth International Congress on Glass (Kyoto, Japan: The Ceramic Society of Japan, 1974), 23-30.

6. H. Richter, "Crack Propagation in Glass Under Liquids in an Intermediate Range of Crack Velocities", Strength of Inorganic Glass, ed. C. R. Kurkjian (Plenum Publishing Corp., 1985), 219-229.

7. J. H. Henry, "Energie d'Avancement de Fissure, G, pour une Plaque Percee d'un Trou Soumise en Compression', Mechanics Research Communications, 10 (5) (1983) 253-257.

8. C. G. Sammis and M. F. Ashby, "The Failure of Brittle Porous Solids Under Compressive Stress States", Act Metall., 34 (1986) 511-526.

9. W. E. Warren, "Theoretical Analysis of the Double Cleavage Drilled Compression Specimen", Int. Journal of Fracture, 33 (1987) 223-325.

10. H. Tada, P. C. Paris, and G. R. Irwin, The Stress Analysis of Cracks Handbook (Hellertown, PA: Del Research Corp., 1973).

SECURITY CLASSIFICATION OF THIS PAGE (When Data Entered)

REPORT DOCUMENTATION PAGE

READ INSTRUCTIONS BEFORE COMPLETING FORM

1. REPORT NUMBER

2. GOVT ACCESSION NO.

3. RECIPIENT'S CATALOG NUMBER

4. TITLE (and Subtitle)

Mechanical Property Enhancement in Ceramic Matrix Composites

5. TYPE OF REPORT & PERIOD COVERED

Interim Report

6. PERFORMING ORG. REPORT NUMBER

7. AUTHOR(s)

S. W. Freiman, T. W. Coyle, E. R. Fuller Jr., P. L. Swanson, D. C. Cranmer, and W. Haller

8. CONTRACT OR GRANT NUMBER(s)

N00014-86-F-0096

9. PERFORMING ORGANIZATION NAME AND ADDRESS

National Bureau of Standards, Gaithersburg, MD
Drexel University, Philadelphia, PA

10. PROGRAM ELEMENT, PROJECT, TASK AREA & WORK UNIT NUMBERS

11. CONTROLLING OFFICE NAME AND ADDRESS

SDIO/IST
Washington, D.C.

12. REPORT DATE

April 30, 1988

13. NUMBER OF PAGES

55

14. MONITORING AGENCY NAME & ADDRESS (if different from Controlling Office)

Office of Naval Research
800 N. Quincy Street
Arlington, VA 22217

15. SECURITY CLASS. (of this report)

15a. DECLASSIFICATION/DOWNGRADING SCHEDULE

16. DISTRIBUTION STATEMENT (of this Report)

17. DISTRIBUTION STATEMENT (of the abstract entered in Block 20, if different from Report)

18. SUPPLEMENTARY NOTES

19. KEY WORDS (Continue on reverse side if necessary and identify by block number)

ceramics; composites; fibers; fracture; interfacial strength

20. ABSTRACT (Continue on reverse side if necessary and identify by block number)

The interfacial strength between AVCO SCS-6 filaments and a borosilicate glass matrix was measured using an indentation push-in technique. Crack-filament interactions were investigated using a fracture mechanics technique (DCDC). An ultraviolet curing technique, coupled with hot pressing was developed to prepare SiC filament-borosilicate glass composites.

DD FORM 1 JAN 73 1473 EDITION OF 1 NOV 65 IS OBSOLETE
S/N 0102-LF-014-6601

SECURITY CLASSIFICATION OF THIS PAGE (When Data Entered)

NBS-114A (REV. 2-8C)

U.S. DEPT. OF COMM. **BIBLIOGRAPHIC DATA SHEET** *(See instructions)*	1. PUBLICATION OR REPORT NO. NBSIR 88-3798	2. Performing Organ. Report No.	3. Publication Date APRIL 1988

4. TITLE AND SUBTITLE

Mechanical Property Enhancement in Ceramic Matrix Composites.

5. AUTHOR(S) S. W. Freiman, T. W. Coyle, E. R. Fuller Jr., P. L. Swanson, D. C. Cranmer, and W. Haller

6. PERFORMING ORGANIZATION *(If joint or other than NBS, see instructions)*

NATIONAL BUREAU OF STANDARDS
U.S. DEPARTMENT OF COMMERCE
GAITHERSBURG, MD 20899

7. Contract/Grant No.

8. Type of Report & Period Covered

9. SPONSORING ORGANIZATION NAME AND COMPLETE ADDRESS *(Street, City, State, ZIP)*

10. SUPPLEMENTARY NOTES

☐ Document describes a computer program; SF-185, FIPS Software Summary, is attached.

11. ABSTRACT *(A 200-word or less factual summary of most significant information. If document includes a significant bibliography or literature survey, mention it here)*

The interfacial strength between AVCO SCS-6 filaments and a borosilicate glass matrix was measured using an indentation push-in technique. Crack-filament interactions were investigated using a fracture mechanics technique (DCDC). An ultraviolet curing technique, coupled with hot pressing was developed to prepare SiC filament-borosilicate glass composites.

12. KEY WORDS *(Six to twelve entries; alphabetical order; capitalize only proper names; and separate key words by semicolons)*

ceramics; composites; fibers; fracture; interfacial strength

13. AVAILABILITY

☒ Unlimited

☐ For Official Distribution. Do Not Release to NTIS

☐ Order From Superintendent of Documents, U.S. Government Printing Office, Washington, D.C. 20402.

☒ Order From National Technical Information Service (NTIS), Springfield, VA. 22161

14. NO. OF PRINTED PAGES

60

15. Price

$13.95

IR 88-3799

CANCELLED 03/16/90

UNAVAILABLE FOR BINDING